HHS Public Access

Author manuscript

Neuron. Author manuscript; available in PMC 2023 April 20.

Published in final edited form as:

Neuron. 2022 April 20; 110(8): 1416–1431.e13. doi:10.1016/j.neuron.2022.01.019.

Hippocampal-Amygdala Memory Circuits Govern Experience-Dependent Observational Fear

Joseph I. Terranova[1], **Jun Yokose**[1], **Hisayuki Osanai**[1], **William D. Marks**[1], **Jun Yamamoto**[1], **Sachie K. Ogawa**[1], **Takashi Kitamura**[1,2,3,*]

[1]Department of Psychiatry, University of Texas Southwestern Medical Center, Dallas, Texas, 75390, USA

[2]Department of Neuroscience, University of Texas Southwestern Medical Center, Dallas, Texas, 75390, USA

[3]Lead Contact

Summary

The empathic ability to vicariously experience the other's fearful situation, a process called observational fear (OF), is critical to survive in nature and function in society. OF can be facilitated by both prior similar fear experience in the observer and social familiarity with the demonstrator. However, the neural circuit mechanisms of experience-dependent OF (Exp OF) remain unknown. Here, we demonstrate that hippocampal-basolateral amygdala (HPC-BLA) circuits in mice, without involving anterior cingulate cortex, considered a center of OF, mediate Exp OF. Dorsal HPC neurons generate fear memory engram cells in BLA encoding prior similar fear experience, which are essential for Exp OF. On the other hand, ventral HPC neurons respond to the familiar demonstrator's aversive situation during Exp OF, which reactivate the fear memory engram cells in BLA to elicit Exp OF. Our study provides new insight for the memory engram-dependent perception-action coupling that underlies empathic behaviors like Exp OF.

Graphical Abstract

*Correspondence: Takashi.Kitamura@UTSouthwestern.edu.

Author Contributions

J.T., and T.K., contributed to the study design. J.T., J.Yo., and H.O. conducted the surgeries, behavior, and histological experiments. W.M conducted ex vivo electrophysiology experiments. J.T conducted in vivo calcium imaging experiments. J.Yo conducted the AAV production. J.T, J.Yo., H.O., W.M., J.Ya., S.O., and T.K., contributed to the interpretation for data analyses. J.T., and T.K., wrote the paper. All authors approved the final manuscript.

Declaration of Interests

The authors declare no competing interests.

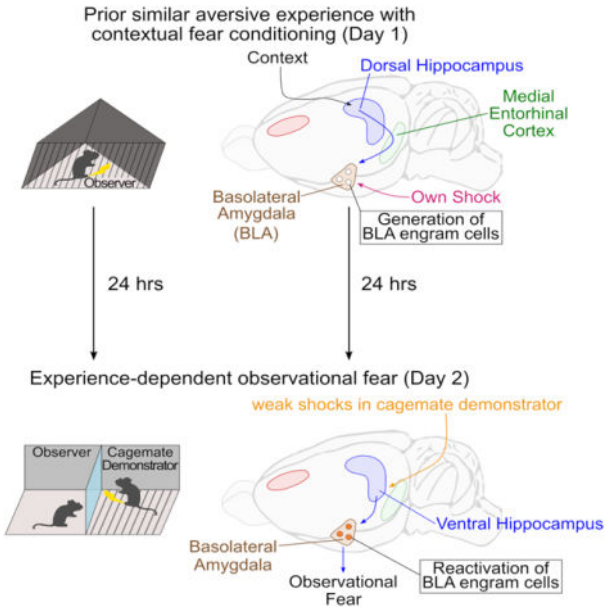

Short Summary

How do prior similar experiences and social familiarity with the demonstrator facilitate observational fear? In this study, Terranova et al. find that memory engram circuits in the hippocampal-amygdala networks encoding prior experiences integrate a perception-action coupling for experience-dependent enhancement of observational fear.

Introduction

Fear, an emotion triggered by danger or threat, is essential for survival (Adolphs, 2013; LeDoux, 2012). Fear can be acquired either by direct experience or indirect experience through social observation (Barrett et al., 2007; Olsson and Phelps, 2007). The empathic ability to vicariously experience the other's aversive events is called observational fear (OF) (Debiec and Olsson, 2017; Keum and Shin, 2019; Panksepp and Lahvis, 2011), which is critical for observational fear learning (John et al., 1968; Keum and Shin, 2019; Mineka et al., 1984; Olsson and Phelps, 2007) and prosocial behaviors (Ben-Ami Bartal et al., 2011; Burkett et al., 2016; Church, 1959; Hernandez-Lallement et al., 2020; Sato et al., 2015). In OF, an observer witnesses a demonstrator in an aversive situation and responds with fear behaviors. Rodent studies have established behavioral models of OF (Atsak et al., 2011; Chen et al., 2009; Gonzalez-Liencres et al., 2014; Jeon and Shin, 2011; Pereira et al., 2012; Sanders et al., 2013) and identified several neural mechanisms, particularly in the anterior cingulate cortex (ACC) and basolateral amygdala (BLA) networks, which are currently considered to be the center for OF (Allsop et al., 2018; Burgos-Robles et al., 2019; Carrillo et al., 2019; Choi and Jeong, 2017; Ito et al., 2015; Ito and Morozov, 2019; Jeon et al., 2010; Keum et al., 2018; Kim et al., 2014; Kim et al., 2012; Liu et al., 2017; Pisansky et al., 2017; Sakaguchi et al., 2018; Twining et al., 2017).

OF is facilitated by both prior similar fear experience in the observer and social familiarity with the demonstrator (Atsak et al., 2011; Cao et al., 2015; Cruz et al., 2020; Golkar et al., 2015; Gonzalez-Liencres et al., 2014; Jeon et al., 2010; Kim et al., 2010; Lidhar et al., 2017; Mineka et al., 1984; Pisansky et al., 2017; Sakaguchi et al., 2018; Sanders et al., 2013). If the demonstrator's reaction is robust, the observer expresses OF without prior experiences (we refer to this as Naive OF), which has been generally used as a rodent OF model and primarily depends on ACC and BLA (Choi and Jeong, 2017; Jeon et al., 2010; Kim et al., 2019). However, in nature and our lives, the demonstrator's reaction is often ambiguous and thus difficult to understand. To fully understand the other's situation, the observer uses both prior similar fear experience and social familiarity with the demonstrator, which facilitates OF (we refer to this as experience-dependent OF; Exp OF). Exp OF is evolutionarily conserved from rodents to humans (Debiec and Olsson, 2017; Hooker et al., 2008; Keum and Shin, 2019; Monfils and Agee, 2019; Olsson and Phelps, 2007). Recent studies have examined the role of ACC and BLA on Exp OF (Allsop et al., 2018; Carrillo et al., 2019; Han et al., 2019; Smith et al., 2021). However, because these studies delivered strong shock protocols to the demonstrator that are sufficient to induce OF in observers regardless of prior experience, the extent to which the ACC to BLA pathway is involved in Exp OF is still unclear. To clarify this neural mechanism, it would be more desirable to deliver a weak shock protocol to the demonstrator that never induces OF without prior experience.

On the other hand, the hippocampus (HPC), particularly dorsal HPC (dHPC), is crucial for the formation and recall of contextual fear memory to remember own contextual fear experience (Frankland et al., 2006; Hunsaker and Kesner, 2008; Kheirbek et al., 2013; Kim et al., 1993; Kitamura et al., 2009; Kitamura et al., 2015; Maren and Fanselow, 1997; Wiltgen et al., 2006), whereas ventral HPC (vHPC) is crucial for the formation and recall of social recognition memory (Deng et al., 2019; Jimenez et al., 2020; Okuyama et al., 2016). Thus, pre-requisite understanding of others' aversive situations may recruit dorsoventral HPC function to integrate memory information about prior similar fear experience in the observer and social familiarity with the demonstrator to elicit Exp OF. The contribution of HPC to Exp OF, however, remains unknown.

Simulation Theory provides a possible framework for Exp OF, such that the observer understands the demonstrator's situation through an unconscious internal simulation in which the observer puts itself in the demonstrator's situation by recalling memory of a prior similar own experience (Gallese and Goldman, 1998; Gordon, 1986; Heal, 1986). Previous studies suggest that a shared neural population activity may integrate a perception-action coupling for Exp OF (Gallese and Goldman, 1998; Gangopadhyay and Schilbach, 2012; Gibson, 1958; Gibson, 1979; Singer et al., 2004). However, no studies have directly examined the role of shared neural population activity on Exp OF. Recent advances using activity-dependent cell labeling with optogenetics have identified the neural population encoding a specific memory, called memory engram cells, which are a subpopulation of neurons that undergo biological changes during an experience and encode a specific episode (Josselyn and Tonegawa, 2020; Kandel et al., 2014; Liu et al., 2012; Silva et al., 2009). Since memory engram cells for contextual fear memory have been found in several brain regions including dHPC and BLA (Choi et al., 2018; Kitamura et al., 2017; Tonegawa et al.,

2015; Tonegawa et al., 2018), we speculate that memory engram cells encoding prior similar fear experience may work as an integrator of perception-action coupling to elicit Exp OF.

In this study, we first established two models of OF in mice: Naive OF, which does not require prior experience to induce OF, and Exp OF, which requires prior similar fear experience and social familiarity with the demonstrator to induce OF. Next, we investigated how ACC, BLA, dHPC and vHPC activity and the relationship across these brain regions contributes to Exp OF and Naive OF. We demonstrate that dorsoventral HPC to BLA pathways, without ACC, are crucial for Exp OF, while the ACC to BLA pathway is essential for Naive OF. Second, to understand the neural mechanisms about how the HPC-BLA networks mediate Exp OF, we addressed the role of memory engram cells in dHPC and BLA that encode prior similar own fear experience on Exp OF. We found that fear memory engram cells in BLA are reactivated during and are necessary for Exp OF. Dorsal HPC neurons generate fear memory engram cells in BLA during prior own fear experience, while ventral HPC neurons respond to the familiar demonstrator's fearful situation, which reactivate fear memory engram cells in BLA to elicit Exp OF. Finally, *in vivo* calcium imaging revealed that the fear memory engram cells in BLA are activated during both own and the familiar demonstrator's aversive moment. Therefore, we propose that memory engram circuits in the HPC-BLA govern the integration of perception-action coupling as a principle of Exp OF.

Results

Naive and Exp OF behavioral models

We established two models of OF in mice: Naive OF (Jeon et al., 2010; Keum et al., 2018; Twining et al., 2017), which does not require prior experience to induce OF (Figure 1A, 1D–F, S1A–F), and Exp OF (Atsak et al., 2011; Sakaguchi et al., 2018; Sanders et al., 2013), which requires prior similar fear experience with contextual fear conditioning (CFC) and social familiarity (SF) with the demonstrator to induce OF (Figure 1B, 1G–I, S2). For both models, the OF apparatus consists of two chambers separated by a transparent plexiglass partition. The observer chamber has a plexiglass floor, and the demonstrator chamber has an exposed stainless-steel rod floor to deliver electrical footshocks. In Naive OF (Figure 1A), after a habituation period (HP), the strong OF protocol (sOF/S) was applied to the demonstrator during the shock period (SP), which produced a robust demonstrator's fear reaction (Figure 1C, S1F) and then induced the freezing response in the observer (Figure 1D–F, S1C–D). Naive OF was diminished when visual inputs were blocked by an opaque partition (Figure 1D–F, 1J), as previously reported (Hong and Choi, 2018; Jeon et al., 2010). Object-threat stimulation, which induces non-social visual and auditory stimuli equivalent to the sOF protocol, did not induce a comparable observer freezing response (Figure S1A–D). These indicate that Naive OF requires a socially-induced visual perception stimulus. In Exp OF (Figure 1B), on Day 1, observers received CFC in a different chamber as prior similar fear experience. On Day 2, after a habituation period, the weak OF protocol (wOF/W) was applied to the demonstrator, which produced an ambiguous reaction in the demonstrator (Figure 1C, S1F) and induced observer freezing (Figure 1G–I, S2). Exp OF required both CFC experience in the observer and social familiarity with the demonstrator (Figure 1G–I,

S2). In contrast to Naive OF, Exp OF was partially reduced by an opaque partition (Figure 1G–J, S2), indicating that visual stimulation from the demonstrator partially plays a role in Exp OF. Since observer freezing in Exp OF without visual perception was still aligned with the demonstrator's shock moment (Figure 1I, S2B), auditory stimulation from the demonstrator during the shock moment may also facilitate Exp OF (Atsak et al., 2011; Kim et al., 2010). Furthermore, observer freezing level was significantly greater in Exp OF with an opaque partition (W_{opaque}/+/+ group) compared with CFC experience observers tested with a stranger demonstrator (W/+/− group) (Figure 1H), suggesting that observers recognize the familiar demonstrator without visual cues, likely through unique volatile pheromones linked to major urinary proteins of the demonstrator (Cheetham et al., 2007; Hurst et al., 2001; Roberts et al., 2018). Thus, unlike Naive OF, Exp OF is facilitated by a socially-induced multisensory perception, including visual, auditory and olfactory stimulation. With the exception of observers tested with an opaque partition (S_{opaque}/−/− and W_{opaque}/+/+ groups), observers visually attended to the demonstrator during shock delivery (Figure 1K, S1E).

We further examined whether the onset of the observer's freezing response during Naive OF and Exp OF is triggered by the state (freezing behavior) of the demonstrator or by the aversive event in the demonstrator (shock delivery). The freezing state of the demonstrator did not trigger the observer's freezing response, nor did the observer and demonstrator synchronize their freezing behavior (Figure S1G–H). The aversive event in the demonstrator, however, significantly triggered the freezing response in the observer (Figure S1G–H). Therefore, both Naive OF and Exp OF are triggered by the aversive event in the demonstrator, and not the state of the demonstrator.

Roles of ACC and BLA in Exp and Naive OF

Using the Exp OF and Naive OF models (Figure 1), we examined the role of the ACC to BLA pathway by optogenetically inhibiting ACC terminals at BLA in Exp OF or Naive OF (Figure 2A–H). We bilaterally injected either adeno-associated virus 2/5 ($AAV_{2/5}$)-CaMKIIα:eArchT-eYFP or $AAV_{2/5}$-CaMKIIα:eYFP as a control in ACC, implanted optical fibers targeting BLA, and then inhibited the axonal terminals of ACC neurons either during shock delivery to the demonstrator or during the shock interval (Figure 2A–C, 2F). Consistent with previous reports (Jeon et al., 2010; Kim et al., 2021), we found that the ACC to BLA pathway is essential for observer freezing in Naive OF, particularly during the demonstrator's shock moment (Figure 2D–E). Surprisingly, optogenetic terminal inhibition of ACC neurons at BLA in Exp OF did not affect observer freezing (Figure 2G–H). We confirmed these findings by chemical lesion of ACC or BLA prior to Naive OF or Exp OF (Figure S3A–H). Next, we quantified expression of the immediate early gene Arc (activity-regulated cytoskeleton-associated protein (Bramham et al., 2008; Guzowski et al., 1999; Lyford et al., 1995)) after Exp OF or Naive OF (Figure 2I–L, S3I). Arc positivity was higher in Naive OF compared with the non-shock group for both ACC and BLA (Figure 2J). Arc positivity in ACC was not elevated in Exp OF compared with the non-shock group, but was elevated in BLA (Figure 2L). Since a previous report found that functional connectivity and neural oscillatory activity is increased in ACC and BLA at the theta rhythm frequency (4–7 Hz) during Naive OF (Jeon et al., 2010), we examined *in vivo* local field potential

recording from both ACC and BLA during Exp OF. In contrast to Naive OF (Jeon et al., 2010), there was no difference in theta power at the 4–12 Hz frequency and synchrony in ACC and BLA between the habituation and shock period during Exp OF (Figure 2M–O, S4), suggesting that functional connectivity between ACC and BLA during Exp OF is weaker than during Naive OF. These results show that BLA is necessary for both Exp OF and Naive OF, whereas ACC is necessary for Naive OF but dispensable for Exp OF.

Roles of dorsoventral hippocampus in Exp and Naive OF

Next, we examined the role of dorsoventral HPC activity on Exp OF and Naive OF using chemogenetic neural silencing of dHPC or vHPC by injecting $AAV_{2/8}$-CaMKIIα:hM4Di-mCherry or $AAV_{2/8}$-CaMKIIα:mCherry as a control (Figure 3A–B). Inhibition of dHPC, but not vHPC, during CFC on Day 1 impaired observer freezing in Exp OF on Day 2 compared with the mCherry group (Figure 3G–I). On the other hand, inhibition of vHPC, but not dHPC, during wOF impaired observer freezing in Exp OF compared with the mCherry group (Figure 3J–L). dHPC or vHPC inhibition did not affect observer freezing in Naive OF (Figure 3M–O). We confirmed that CNO reduced neural activity of hM4Di-expressing neurons in dHPC and vHPC *in vitro* (Figure 3C–F) and *in vivo* (Figure S5A–B). CNO injection on Day 1 or Day 2 without the expression of hM4Di did not affect observer freezing during Exp OF (Figure S5C–F). Importantly, we observed that prior experience (CFC experience and social familiarity with the demonstrator) enhanced observer freezing during Exp OF even when using the strong OF protocol (Figure S6A–B), and this enhancement required vHPC (Figure S6C–E), indicating that vHPC activity is necessary for Exp OF irrespective of OF protocols. These data show that there are differential contributions of dorsoventral HPC on Exp OF; dHPC activity is necessary for Exp OF during CFC on Day 1, while vHPC activity is necessary for Exp OF during wOF on Day 2.

Based on contributions of BLA (Figure 2, S3) and dorsoventral HPC activity to Exp OF (Figure 3), we examined the roles of dHPC or vHPC activity on Arc expression in BLA during CFC or Exp OF. We injected $AAV_{2/8}$-CaMKIIα:hM4Di-mCherry or $AAV_{2/8}$-CaMKIIα:mCherry into dHPC or vHPC and examined Arc expression in BLA after CFC or Exp OF. CFC increased Arc positivity in BLA compared with the homecage group, and the enhancement of Arc positivity by CFC was reduced by dHPC inhibition (Figure 4A–B). While Exp OF also increased Arc positivity in BLA, the enhancement by Exp OF was reduced by vHPC inhibition (Figure 4C–D), indicating that the enhancements of BLA activity by CFC and Exp OF are differentially regulated by the dorsoventral HPC activity.

Role of BLA fear memory engram cells in Exp OF

To understand the neural mechanisms about how the HPC-BLA networks mediate Exp OF, we examined the roles of fear memory engram cells in HPC and BLA encoding prior similar own fear experience on Exp OF (Figure 4E), by selectively labeling the subpopulation of BLA or dHPC CA1 (dCA1) neurons activated during CFC using doxycycline-off (off-Dox) activity-dependent cell tagging with the Robust Activity Marking (RAM) system (Sorensen et al., 2016; Sun et al., 2020). The RAM system directly couples the human c-fos minimal promoter with four tandem repeats of an enhancer module (PRAM) to the destabilized tetracycline transactivator (d2tTA), a key component of the doxycycline (Dox) system for

inducible expression of a gene of interest. We injected mice with $AAV_{2/9}$-PRAM:d2tTA-TRE:NLS-mKate2 into BLA or dCA1. On Day 1, we subjected mice to CFC under off-Dox condition, and then to Exp OF or exposure to conditioned context (CTX) on Day 2 (Figure 4E). Neurons activated by CFC were labeled with mKate2, and neurons activated by Exp OF or CTX were labeled with Arc antibody (Figure 4F, 4I, S7A). There was no mKate2 expression in the on-Dox control groups (Figure 4F, 4I). In the CTX group, consistent with previous reports (Cai et al., 2016; Kitamura et al., 2017; Redondo et al., 2014; Roy et al., 2019; Tanaka et al., 2018) Arc positivity was higher in $mKate2^+$ compared with $mKate2^-$ neurons in both BLA and dCA1 (Figure 4G, 4J, Table S2C). In the Exp OF group, Arc positivity was higher in $mKate2^+$ compared with $mKate2^-$ neurons in BLA and lower in dCA1, indicating that the subpopulation of BLA neurons activated during CFC was reactivated during Exp OF (Figure 4H, Table S2A), whereas the subpopulation of dCA1 neurons was not reactivated (Figure 4K, Table S2A). There was no significant enhancement of Arc expression in CFC-activated ACC or vHPC CA1 (vCA1) neurons during Exp OF (Table S2A). Critically, when we conduct wOF on Day 1 and CFC on Day 2, the subpopulation of BLA neurons activated during wOF was not reactivated during CFC (Figure S8), indicating that overlapping neural ensemble activation in BLA during Exp OF is CFC experience-dependent.

To directly examine the role of the subpopulation of BLA neurons activated during CFC on Exp OF, we injected $AAV_{2/9}$-PRAM:d2tTA-TRE:HA-hM4Di or $AAV_{2/9}$-PRAM:d2tTA-TRE:NLS-mKate2 as a control into BLA to express HA-hM4Di or mKate2 in neurons activated during CFC, and then inhibited the subpopulation activity during Exp OF or CTX (Figure 5A–D, S7B–E). Consistent with previous reports (Kitamura et al., 2017; Redondo et al., 2014), hM4Di-induced neural silencing of the BLA subpopulation activated during CFC impaired freezing response during CTX compared with the mKate2 control group (Figure 5C), indicating that the BLA subpopulation activated during CFC is defined as memory engram cells, which encodes CFC memory (Josselyn and Tonegawa, 2020; Kandel et al., 2014; Silva et al., 2009). In the Exp OF group, hM4Di-induced inhibition of the BLA subpopulation activated during CFC impaired observer freezing during Exp OF compared with the mKate2 control (Figure 5D, S7D–E). To verify that the BLA fear memory engram cells formed during CFC are specifically required for Exp OF, we injected $AAV_{2/9}$-PRAM:d2tTA-TRE:HA-hM4Di or $AAV_{2/9}$-PRAM:d2tTA-TRE:NLS-mKate2 as a control into BLA to express HA-hM4Di or mKate2 in neurons, subjected mice to CFC, and then labeled BLA neurons that were activated by an unrelated aversive experience (bright light illumination on an elevated platform, see Methods) (Figure 5E). Critically, inhibition of the subpopulation of BLA neurons labeled during an unrelated aversive experience did not affect observer freezing during Exp OF (Figure 5F), nor was this subpopulation of neurons reactivated by Exp OF (Figure 5G). These data indicate that fear memory engram cells in BLA encoding prior similar own fear experience are specifically reactivated during Exp OF and are specifically necessary for Exp OF.

To investigate temporal dynamics of fear memory engram cell activity in BLA in Exp OF, we examined longitudinal *in vivo* calcium imaging by injecting $AAV_{2/5}$-CaMKIIα:GCaMP6f into BLA to express GCaMP6f, a calcium indicator, in excitatory neurons and imaged through a head-mounted miniature fluorescent microscope during CFC

(Day 1) and Exp OF (Day 2) (Figure 5H–5I, S9A–B, N=160 neurons/5 mice). Consistent with previous studies (Corder et al., 2019; Zhang et al., 2020), a small fraction of BLA neurons (23.75%) showed a significant increase in Ca^{2+} activity after footshock delivery during CFC on Day 1 (Figure S9C–D), which we refer to as CFC shock-responding (SR) cells. Because the proportion of CFC SR cells in BLA positively correlates with freezing behavior (Zhang et al., 2020) and the CFC SR cells are significantly reactivated during freezing response in the conditioned context (Zhang et al., 2020), we consider the CFC SR cells to be fear memory engram cells, whereas we categorize the remaining BLA neurons as CFC other cells (Figure S9C–D). On Day 2, we observed OF SR, shock-suppressed (SS), and non-shock responding (NSR) cells during Exp OF (Figure 5J and Figure S9E–G). We found a higher proportion of CFC SR cells were reactivated during a familiar demonstrator's shock moments compared with the CFC other cells (55.0% vs. 35.0%, Figure 5K). Conversely, a lower proportion of CFC SR cells were suppressed during a familiar demonstrator's shock moments compared with the CFC other cells (8.0% vs. 29.0%, Figure 5K). These results, combined with Arc activation data (Figure 4G–H, 5A–G), suggest that the BLA fear engram cells exhibit a perception-action neural activity by responding during own shock moment as well as the familiar demonstrator's shock moment.

Role of vHPC-BLA pathway in Exp OF

To examine the role of vHPC on the reactivation of fear memory engram cells in BLA during Exp OF, we injected $AAV_{2/9}$-PRAM:d2tTA-TRE:NLS-mKate2 into BLA and simultaneously injected $AAV_{2/8}$-CaMKIIα:hM4Di-mCherry or $AAV_{2/8}$-CaMKIIα:mCherry into vHPC. We labeled fear memory engram cells with mKate2 using the off-Dox condition during CFC and injected CNO 30 minutes before wOF (Figure 6A). We found no difference in Arc positivity between $mKate2^+$ and $mKate2^-$ neurons in BLA of the hM4Di group, whereas Arc positivity was significantly higher in $mKate2^+$ than $mKate2^-$ neurons in BLA of the mCherry group (Figure 6B–C, S7F). We also found there was no difference in Arc positivity between $mKate2^+$ and $mKate2^-$ neurons in BLA when using a non-shocked familiar demonstrator or shocked stranger demonstrator (Figure 6D–E, S7G, Table S2B). These indicate that vHPC activity is essential for reactivation of fear memory engram cells in BLA during Exp OF, and both demonstrator's shock stimuli and social familiarity are required for this reactivation.

To characterize the dominant feature of vHPC CA1 (vCA1) neuron activity in Exp OF, we examined longitudinal *in vivo* calcium imaging by injecting $AAV_{2/5}$-CaMKIIα:GCaMP6f into the vCA1 region to record from excitatory neurons in vCA1 during Exp OF on Day 2 with a familiar demonstrator and OF with a stranger demonstrator on Day 3 (Figure 6F, N=153 neurons/4 mice). We found a larger proportion of OF shock-responding cells with a familiar demonstrator compared with that with a stranger demonstrator (Figure 6G–H). However, there was no overlap between OF shock-responding cells with a familiar or a stranger demonstrator (Figure 6I). These indicate that the subset of vHPC CA1 neurons selectively respond to the shock moment in the familiar demonstrator during Exp OF.

To clarify whether BLA-projecting vHPC neurons respond to the familiar demonstrator's aversive situation, we examined Arc expression in BLA-projecting vHPC neurons after Exp

OF with a familiar or stranger demonstrator by injecting a retrograde tracer, cholera toxin subunit B (CTB), into BLA (Figure 7A–B). Arc positivity in CTB^+ neurons in vHPC of the familiar demonstrator group was higher than the stranger demonstrator group (Figure 7B, Table S2D), while there was no significant difference in BLA-non projecting (CTB^-) vHPC neurons (Figure 7B). Next, we examined optogenetic inhibition of vHPC terminals in BLA by injecting $AAV_{2/5}$-CaMKIIα:eArchT-eYFP or $AAV_{2/5}$-CaMKIIα:eYFP as a control in vHPC and implanting optical fibers targeting BLA (Figure 7C–D). Inhibition of vHPC terminals in BLA during the shock delivery period reduced observer freezing in Exp OF (Figure 7D).

Because vHPC to BLA input during observation of shock delivery to the familiar demonstrator is necessary for observer freezing in Exp OF (Figure 7D), we hypothesized that BLA-projecting vHPC neurons specifically access BLA fear memory engram cells to facilitate observer freezing in Exp OF. To test this hypothesis, we injected $AAV_{2/5}$-CaMKIIα:eArchT-eYFP or $AAV_{2/5}$-CaMKIIα:eYFP as a control in vHPC, injected $AAV_{2/9}$-PRAM:d2tTA-TRE:NLS-mKate2 in BLA, and implanted optical fibers targeting BLA (Figure 7E–F). We labeled BLA fear memory engram cells during CFC with mKate2, optogenetically inhibited vHPC terminals at BLA during shock delivery to the demonstrator in Exp OF, and then examined the reactivation of BLA fear memory engram cells during Exp OF. Although BLA fear memory engram cells were significantly reactivated during Exp OF in both eYFP and eArchT groups, we found the strength of this reactivation was greater in the eYFP group (Figure 7G–H, 7K). Optogenetic terminal inhibition of vHPC neurons at BLA in Exp OF reduced Arc expression in the $mKate2^+$ neurons but not $mKate2^-$ neurons in BLA (Figure 7I–J), indicating that BLA-projecting vHPC neurons are specifically accessing the BLA fear memory engram cells during Exp OF. Taken together, these results indicate that BLA-projecting vHPC neurons respond to the familiar demonstrator's aversive moment, which directly reactivates BLA fear engram cells for the expression of Exp OF.

Discussion

In this study, we found that HPC to BLA pathways, without ACC, facilitate Exp OF (Figure 8B–C), while the ACC to BLA pathway mediates Naive OF (Figure 8A). The two distinct neural pathways for Exp OF and Naive OF are differentially evoked by a multisensory perception stimulus including visual, auditory and olfactory modalities or mainly a visual perception stimulus, respectively, during the demonstrator's shock moment. dHPC neurons are necessary for the generation of fear memory engram cells in BLA encoding CFC memory on Day 1 (Figure 8B). The fear memory engram cells in BLA are reactivated during Exp OF and the reactivation is necessary for Exp OF on Day 2 (Figure 8C). On the other hand, vHPC neurons respond to the familiar demonstrator's fearful situation that reactivate the fear memory engram cells in BLA to elicit Exp OF on Day 2 (Figure 8C). BLA fear engram cells are activated during both own shock and the familiar demonstrator's shock moment (Figure 8B–C). The two distinct neural pathways for Exp OF and Naive OF facilitate OF in a parallel manner (Figure 8D).

Our model introduces 3 new concepts. First, HPC-BLA circuits mediate Exp OF. Previous studies hypothesized that prior experience may enhance ACC activity, which could induce Exp OF by using a strong shock protocol (Allsop et al., 2018; Carrillo et al., 2019; Keum and Shin, 2019; Sakaguchi et al., 2018). In contrast, we specifically targeted Exp OF (Figure 1) by a using weak shock protocol that never induces OF without prior experience and found that both CFC and social familiarity do not change ACC activity during Exp OF, and that ACC is dispensable for Exp OF (Figure 2, S3, Table S2A, 2D), while the ACC to BLA pathway is crucial for Naive OF (Figure 2, S3). Instead, HPC to BLA pathways facilitate Exp OF (Figure 3). These two distinct neural pathways for Exp OF and Naive OF are evoked by different sensory perception modalities (Figure 1D–J, S2). Furthermore, when we examined Exp OF using the strong shock protocol, as previously demonstrated (Allsop et al., 2018; Carrillo et al., 2019; Han et al., 2019; Smith et al., 2021), we found that both ACC and vHPC are crucial for Exp OF with the strong shock protocol (Figure S6, S13). These findings indicate that it is possible the ACC-BLA pathway and the HPC-BLA pathway parallelly facilitate OF (Fig. 8D), which may allow individuals to have more adaptive empathic ability in different social situations (Morelli et al., 2014).

Second, fear memory engram cells in BLA encoding prior similar own fear experience are reactivated during Exp OF and are necessary for Exp OF. Empathic ability is considered to be based on a perception-action coupling (Gangopadhyay and Schilbach, 2012; Gibson, 1958; Gibson, 1979), such that observing the other's fear experience activates the shared neural ensemble activity with prior similar fear experience, which in turn elicits the observational fear response (Gallese and Goldman, 1998). Calcium imaging and activity-dependent cell tagging in BLA showed that neurons activated during own shock moment are reactivated during the familiar demonstrator's shock moment in Exp OF (Figure 4H, 5A–D, 5H–K, Table S2A). On the other hand, the neural ensemble activated by an unrelated aversive experience was neither reactivated during Exp OF nor was necessary for Exp OF (Figure 5E–G). These indicate that the BLA fear memory engram cells integrate the perception-action coupling for Exp OF.

We further demonstrated the circuit mechanisms about how HPC networks generates and reactivates the fear memory engram cells during Exp OF. Since CFC experience, rather than immediate shock experience, is required for Exp OF as well as Arc expression in BLA during CFC (Figure S11), dHPC neurons may send contextual information via subiculum and/or entorhinal cortex (Kitamura et al., 2017; Kitamura et al., 2014; Roy et al., 2017) and, simultaneously, the thalamus sends its own footshock information during CFC (Pellman and Kim, 2016) to generate fear memory engram cells in BLA encoding CFC memory on Day 1 (Figure 8B). Although, the role of dHPC in Exp OF may be limited depending on the protocol used for own fear experience (Figure S10A–C). After the generation, vHPC neurons, instead of dHPC neurons, reactivate the BLA fear memory engram to elicit Exp OF (Figure 8C), irrespective of own shock protocols (Figure S10D–F). While vHPC neurons divergently project to regions other than BLA, including the medial prefrontal cortex, nucleus accumbens, and other subregions of the amygdala (Bazelot et al., 2015; Ciocchi et al., 2015; Hübner et al., 2014; Kim and Cho, 2017), we found no evidence that vHPC projections, other than BLA, are necessary Exp OF (Figure S12), indicating that vHPC-BLA pathway is specifically crucial for Exp OF. In the vHPC-BLA pathway,

there are multiple projections; the direct pathway, from vCA1 pyramidal neurons to BLA pyramidal neurons (Bazelot et al., 2015; Hübner et al., 2014; Kim and Cho, 2017, 2020), and the feedforward inhibition pathway, from vCA1 pyramidal neurons to BLA pyramidal neurons via BLA inhibitory neurons (Bazelot et al., 2015; Graham et al., 2021; Hübner et al., 2014; Kim and Cho, 2017, 2020). Since the feedforward inhibition is driven when vHPC neurons are activated at theta range (Bazelot et al., 2015; Graham et al., 2021), it is necessary to examine the nature of vHPC population activity during Exp OF. To examine the neural activity in vHPC, we measured the LFP from vHPC and observed a significant reduction in LFP power at theta (7.5–9 Hz) in vHPC during Exp OF compared with the habituation period (Figure S4C), while only a subpopulation of vHPC neurons is preferentially activated during demonstrator's shock moment (Figure 6G–I). We also found that optogenetic terminal inhibition of vHPC neurons at BLA during the demonstrator's shock moments inhibited Arc expression in the BLA fear memory engram cells during Exp OF (Figure 7I, 7K), and inhibited observer freezing response as well during Exp OF (Figure 7D). These results clearly show that vHPC pyramidal neurons directly activate the subset of BLA pyramidal neurons that encode prior own fear experience during Exp OF. Together, the HPC-BLA memory engram circuits induce the perception-action coupling by activating the fear memory engram cells in BLA via dorsoventral HPC regulation for Exp OF, as predicted by Simulation Theory (Gallese and Goldman, 1998; Gordon, 1986).

A recent study found that a subset of ACC neurons shows a perception-action neural mechanism that responds to own shock moment as well as the demonstrator's shock moment during strong (1.5 mA shock), but not weak (0.4 mA shock), OF protocol in rats (Carrillo et al., 2019), which is consistent with our Arc experiment (Figure 2I–L). Since the fear memory engram cells in BLA can respond to both own shock moment and the demonstrator's shock moment during weak OF protocol for Exp OF, we speculate that the perception-action activity in ACC neurons and the BLA memory engram cells would trigger Naive OF, Exp OF or both, depending on the social contexts.

Third, we demonstrate how social familiarity with the demonstrator facilitates Exp OF. Self-Expansion Theory suggests (Andersen and Chen, 2002; Aron et al., 1998; Aron and Aron, 1996; Beckes et al., 2013) that social familiarity enhances the overlap of own personality traits, memories and knowledge with familiar others, which may facilitate Exp OF. However, virtually nothing was known about the neural mechanisms. In this study, we demonstrated several findings. vCA1 neurons are more active when a familiar demonstrator receives shocks compared with a stranger demonstrator (Figure 6H). Since there was no significant overlap between OF SR cells in vCA1 on Day 2 with a cagemate demonstrator and Day 3 with a stranger demonstrator (Figure 6I), OF SR cell activity may be facilitated by the social memory engram cells for the familiar demonstrator in vCA1, since a subset of vCA1 neurons encode social memory (Deng et al., 2019; Okuyama et al., 2016). Importantly, we observed a significant activation of BLA-projecting vHPC neurons compared with the BLA-non projecting vHPC neurons during Exp OF (Fig 7A–B), suggesting that social memory engram cells within the population of BLA-projecting vHPC neurons are selectively activated during Exp OF. Next, vHPC activity is essential for reactivation of fear memory engram cells in BLA during Exp OF, and both the demonstrator's shock stimuli and social familiarity are required for this reactivation (Figure 6A–E). Furthermore, vHPC

input into BLA during the familiar demonstrator's shock moment is essential for Exp OF, and this input is necessary for the selective activation of BLA fear memory engram cells, but not non-engram cells, during Exp OF (Figure 7E–K). Together, these findings demonstrate that there is a preferential synaptic connectivity between the two subsets of neurons in vHPC and BLA that differently encode social memory and own fear memory, respectively, which is necessary for in Exp OF.

A final question we addressed is when the preferential connectivity between vHPC and BLA is established to facilitate Exp OF. Given that there are direct monosynaptic connections between vHPC pyramidal neurons and excitatory neurons in the BLA (Bazelot et al., 2015; Hübner et al., 2014; Kim and Cho, 2017, 2020), are there preferential synaptic connections that develop during and/or after CFC between vHPC and BLA to facilitate Exp OF? Because vHPC activity on Day 1 CFC is not necessary for Exp OF (Figure 3I) and because prior own CFC experience does not enhance vHPC Arc expression during Exp OF (Table S2D), we speculated that preferential connections between the sparse populations of neurons in vHPC and BLA develop during Exp OF. To test this possibility, we first considered plasticity within BLA during Exp OF. We injected $AAV_{2/9}$-PRAM:d2tTA-TRE:NLS-mKate2 into BLA, labeled the CFC memory engram cells on Day 1, subjected observers to Exp OF on Day 2, and then subjected observers to Exp OF again on Day 3 and subsequently measured the reactivation of BLA fear memory engram cells (Figure S14A–C). While there was significant reactivation of BLA fear memory engram cells on Day 3 Exp OF, the magnitude of this reactivation was lower compared with reactivation on Day 2 Exp OF (Figure S14B–C). These results suggested neuroplastic changes occur in the BLA fear engram cells during Exp OF. To directly test the necessity of enduring plasticity changes on Exp OF, we injected CPP, a selective and competitive antagonist of N-methyl-D-aspartate (NMDA) receptors, via i.p. injection 30 minutes prior to Exp OF on Day 2, and found that CPP injection impaired observer freezing response (Figure S14D–E). Based on these lines of evidence, we speculate that BLA-projecting vHPC neurons may form the preferential synaptic connection with the BLA fear memory engram cells during Exp OF.

Finally, the potential roles of Exp OF and Naive OF on prosocial behavior remain an open question. Since Exp OF is distinct from Naive OF, not only because of its dependency on self-experience but also because of the involved neural circuit mechanisms and required sensory perceptions, we speculate that Exp OF and Naive OF may have differential contributions in observational fear learning, prosocial behavior or other OF-induced social behaviors (Ben-Ami Bartal et al., 2011; Burkett et al., 2016; Hernandez-Lallement et al., 2020; Sato et al., 2015). While our study does not rule out the potential involvement of other associative cortical regions on Exp OF, our study provides new insight of the memory engram-dependent perception-action coupling as a principle of Exp OF in the HPC-BLA networks. Potentially, this mechanism can be generalized for other types of experience-dependent empathic abilities to vicariously experience the other's situation.

STAR Methods Text

Resource Availability

Lead Contact—Further information and requests for resources and reagents should be directed to and will be fulfilled by the lead contact, Takashi Kitamura (Takashi.Kitamura@UTSouthwestern.edu).

Materials Availability—All data are available in the main text or supplementary materials. Reasonable requests for resources and additional information should be directed to and will be fulfilled by the lead contact.

Data and Code Availability

- All data are available in the main text or supplementary materials, and will be shared by the lead contact upon reasonable request.
- All original code has been deposit at Zenodo and is publicly available as of the date of publication. DOIs are listed in the key resources table.
- Any additional information required to reanalyze the data reported in this paper is available from the lead contact upon reasonable request.

Experimental Model and Subject Details—All procedures relating to mouse care and experimental treatments conformed to NIH and Institutional guidelines, and were conducted with the approval of the UT Southwestern Institutional Animal Care and Use Committee (IACUC). All experiments used wildtype male mice of the C57BL/6J background between 9 weeks and 20 weeks old. Mice were group housed with littermates (2 – 5 mice per cage) for a minimum of 7 days prior to experiments in a 12 hr (6am-6pm) light/dark cycle, with food and water available *ad libitum*. For virus-mediated activity-dependent cell labeling experiments, mice were kept on a doxycycline (on-Dox) diet (40 mg/kg, Bio-serv) at least one week prior to stereotaxic surgery and were continuously maintained on the Dox diet except for specified off-Dox days. All experiments were conducted during the light cycle. Mice were randomly assigned to experimental conditions.

Method Details

Behavioral Models of Observational Fear (OF)—The observational fear (OF) apparatus consists of two chambers (24 cm W × 20 cm D × 20 cm H, observer chamber; 6 cm W × 20 cm D × 20 cm H, demonstrator chamber) divided by a transparent plexiglass partition or an opaque partition. The OF apparatus was inserted into a soundproof fear conditioning chamber (Med Associates). In the observer chamber, there was an opaque plexiglass floor. In the demonstrator chamber, the stainless-steel rod floor was exposed. All behavioral chambers were cleaned between trials with 1.5% Process NPD.

For pilot OF protocols (P1-P4 in Figure S1), two mice (a naive observer and an unfamiliar stranger demonstrator) were individually placed into the observer and demonstrator chambers, respectively, for a 3 minute (protocol 1 and protocol 3) or 5 minute (protocol 2 and protocol 4) habituation period. Subsequently, during the 3 minute demonstrator shock

period, the demonstrator received one of the following four protocols (P1-P4): 1) 0.5 mA, 2-sec foot shock with a 15 second shock interval for a total of 12 shock trials, 2) 0.5 mA, 2-sec foot shock with a 10 second shock interval for a total of 18 shock trials, 3) 1.0 mA, 2-sec foot shock with a 15 second shock interval for a total of 12 shock trials, and 4) 1.0 mA, 2-sec foot shock with a 10 second shock interval for a total of 18 shock trials.

For object-threat stimulation (Object Stim, Object in Figure S1), an object was used to simulate visual and auditory cues generated by the demonstrator during the demonstrator shock period. First, an object (dense fabric ball attached to a string, Diameter; 3 cm, Circumference; 9.42 cm) was placed into the demonstrator chamber. Subsequently, one mouse (a naive observer) was placed into the observer chamber for a 5 minute habituation period. During the habituation period, an experimenter slowly moved the object along the floor of the demonstrator chamber using the attached string to simulate the exploratory behavior of the demonstrator mouse. Next, during the 3 minute object stimulation period, an experimenter manipulated the object to simulate the behavior of the demonstrator mouse during the shock period. Specifically, jumping was simulated by tugging on the object's string 2–4 times (for an average of 3 times) per 10 second object stimulation interval for a total of 18 object stimulation trials. Demonstrator freezing during the shock period was simulated by keeping the object immobile after the simulated jumping. Auditory cues generated during the demonstrator shock period were simulated by the banging of the object on the stainless-steel rod floor during the simulated jumping.

For Naive Observational Fear (Naive OF in Figure 1) (Jeon et al., 2010; Twining et al., 2017), two mice (a naive observer and an unfamiliar stranger demonstrator) were individually placed into the observer and demonstrator chambers, respectively, for a 5 minute habituation period (HP). Subsequently, during the 4 minute demonstrator shock period (SP), the demonstrator received a 1.0 mA, 2-sec foot shock with a 10 second shock interval for a total of 24 shock trials. We refer to the demonstrator shock protocol in Naive OF as strong OF (sOF, S). A subset of observers was subjected to Naive OF with an opaque partition (Figure 1D–F, 1J).

For Experience-Dependent Observational Fear (Exp OF in Figure 1) (Atsak et al., 2011; Gonzalez-Liencres et al., 2014; Sakaguchi et al., 2018; Sanders et al., 2013), on Day 1 a mouse (observer) received prior own similar shock experience by being subjected to contextual fear conditioning (CFC) in Context A (dim white light, black plexiglass triangle inserted into the chamber, chamber scented with 1% acetic acid). The observer was placed into the fear conditioning chamber for a 2 minute habituation period, received a 0.5 mA, 2-sec foot shock, and remained in the fear conditioning chamber for a total of 3 minutes. On Day 2, the observer from Day 1 and a familiar cagemate demonstrator were individually placed into the observer and demonstrator chambers, respectively, in Context B (dim white light, OF apparatus, unscented) for a 3 minute habituation period. Subsequently, during the 3 minute demonstrator shock period, the demonstrator received a 0.5 mA, 2-sec foot shock with a 15 second shock interval for a total of 12 shock trials. We refer to the demonstrator shock protocol in Exp OF as weak OF (wOF, W). A subset of observers was subjected to Exp OF with an opaque partition (Figure 1G–J). Another subset of observers was subjected to Exp OF with the strong OF protocol delivered to the demonstrator (Figure S6, S13).

For all behavioral models of OF, all mice (observers and demonstrators) were separated from their cagemates into an empty holding cage with bedding for 5–35 minutes prior to behavior testing. In situations where there are multiple days of behavior testing (such as in Exp OF), to minimize social transfer of fear, mice were placed back into their holding cages for 30–45 minutes after behavior testing before returning to their respective home cages. For studies requiring timed transcardial perfusions, experimental mice were placed back into their holding cages for 1 hour before starting transcardial perfusions. Because of the large number of OF models and control groups, we applied the following naming convention: Demonstrator Shock Protocol (− = no shock, W = weak OF protocol, S = strong OF protocol) / Observer CFC experience (− = no CFC experience, + = prior experience with CFC in another context) / Demonstrator social familiarity (− = unfamiliar stranger demonstrator, + = familiar cagemate demonstrator). S/−/− is Naive OF and W/+/+ is Exp OF, as shown in the figures. Individual panels for Exp OF / control groups are provided in Figure S2. For auditory fear conditioning (AFC) + Exp OF (Figure S10), observers were subjected to AFC on Day 1. A mouse (observer) received prior own similar shock experience by being subjected to AFC in Context A (as described in the paragraph above). The observer was placed into the chamber and allowed to explore for 100 seconds, at which point a 20 second tone (85 db, 5 kHz) was played and co-terminated with a 0.5 mA, 2-sec foot shock. The observer remained in the chamber for a total of 3 minutes (180 seconds). On Day 2, observers were subjected to Exp OF in Context B, as described in the paragraph above.

Behavioral Analysis of OF—Demonstrator behaviors that were assessed include number of jumps, duration of running, and duration of freezing in response to foot shock. Observer behaviors that were assessed include duration of freezing in both the habituation period (HP) and demonstrator shock period (SP) during OF, and number of gazing epochs to the demonstrator in response to demonstrator shock during OF. We defined a gazing epoch as shock trials in which observers responded by visually attending to the demonstrator. We used gazing epochs as a measure of observer attentiveness to the demonstrator's shock moments. Duration of demonstrator running and duration of demonstrator freezing were reported as percentages during the demonstrator shock period ($\frac{Demonstrator\ running\ or\ freezing\ (s)}{Total\ shock\ period\ duration\ (s)} * 100\%$). Gazing epochs were reported as the overall percentage of gazing epochs out of total shock trials ($\frac{Number\ of\ gazing\ epoch}{Total\ number\ of\ shock\ trials} * 100\%$). Observer freezing during OF in response to demonstrator shock was reported as the percentage of time the observer spent freezing during 1 minute time bins ($\frac{Observer\ freezing\ (s)}{60(s)} * 100\%$), overall percentage of time that the observer spent freezing during the demonstrator shock period ($\frac{Observer\ freezing\ (s)}{Total\ shock\ period\ duration\ (s)} * 100\%$), and the percentage of time that the observer spent freezing during post-shock delivery time bins ($\frac{Observer\ freezing\ during\ a\ specific\ time\ bin\ (s)}{Total\ time\ bin\ duration\ (s)} * 100\%$). We analyzed the observer freezing levels with the interaction analysis by two-way mixed ANOVA between shock delivery effect (habituation period vs. shock period) and experimental treatment applied to the observer. We also analyzed the subtraction freezing level of the observer (percentage of time freezing

during the shock period – percentage of time freezing during the habituation period). Post-shock delivery time bins for 10-sec shock interval protocols were: 0.00 seconds – 3.33 seconds post-shock delivery (bin 1, b1), 3.33 seconds – 6.67 seconds post-shock delivery (bin 2, b2), 6.67 – 10.00 seconds post-shock delivery (bin 3, b3), for a 10-sec shock interval total. Post-shock delivery time bins for 15-sec shock interval protocols were: 0.00 seconds – 5.00 seconds (bin 1, b1), 5.00 seconds – 10.00 seconds (bin 2, b2), 10.00 seconds – 15.00 seconds (bin 3, b3), for a 15-sec shock interval total. To directly compare the effect of an opaque wall on observational fear response in observers during Naive OF and Exp OF, the suppression ratio compared to baseline freezing was calculated for Naive OF observers tested with an opaque partition ($S_{opaque}/-/-$) using the following formula: $\left(\frac{Individual\ Sopaque\ /-/-observer\ freezing\ (s) - Average\ -/-/-observer\ freeezing\ (s)}{Average\ S/-/-observer\ freezing\ (s) - Average\ -/-/-observer\ freezing\ (s)} * 100\%\right)$. The suppression ratio compared to baseline freezing was calculated for Exp OF observers tested with an opaque partition ($W_{opaque}/+/+$) using the following formula: $\left(\frac{Individual\ Wopaque\ /+/+observer\ freezing\ (s) - Average\ -/+/+observer\ freeezing\ (s)}{Average\ W/+/+observer\ freezing\ (s) - Average\ -/+/+observer\ freezing\ (s)} * 100\%\right)$. To determine whether the observer freezing response in Naive OF or Exp OF is triggered by demonstrator freezing response, we examined the occurrence of onset of observer freezing response during demonstrator freezing response epochs and calculated the chance level per mouse with the following formula: $\left(\frac{Demonstrator\ freezing\ (s)}{Total\ shock\ period\ duration\ (s)} * 100\%\right)$. Chance level was then compared with actual occurrence of onset observer freezing response triggered by demonstrator freezing response. To determine whether observer freezing response in Naive OF or Exp OF was triggered by shock delivery moment, we examined the occurrence of onset of observer freezing response during demonstrator's shock moment and calculated the chance level per mouse with the following formula: $\left(\frac{Duration\ of\ shock\ delivery\ to\ to\ the\ demonstrator\ (s)}{Total\ duration\ of\ shock\ interval\ (s)} * 100\%\right)$. Chance level was then compared with the actual occurrence of onset of observer freezing response triggered by shock delivery to the demonstrator. To determine whether the observer and demonstrator synchronize their freezing responses in Naive OF or Exp OF, we calculated the chance overlap index with the following formula: $\left(\frac{Observer\ freezing\ (s)}{Total\ shock\ period\ duration\ (s)} * \frac{Demonstrator\ freezing\ (s)}{Total\ shock\ period\ duration\ (s)} * 100\%\right)$. Chance level overlap was then compared with the actual time the observer and the demonstrator synchronized their freezing response $\left(\frac{Observer\ and\ demonstrator\ synchronized\ freezing\ (s)}{Total\ shock\ period\ duration\ (s)} * 100\%\right)$. Observers that exhibited anxiety during the habituation period (> 20% duration of freezing during the habituation period) were excluded before statistical analysis. All behavior data was recorded and assessed by using the Video Freeze Fear Conditioning System (Med Associates) software and the Behavioral Observation Research Interactive Software (BORIS) (Friard and Gamba, 2016).

Preparation of Adeno-Associated Viruses—$AAV_{2/5}$-CaMKIIα:eArchT3.0-eYFP was acquired from the UNC Vector Core, with a titer of $8.0*10^{12}$ genome copy/mL (#AV4883). $AAV_{2/5}$-CaMKIIα:eYFP was acquired from the UNC Vector Core, with a titer of $5.2*10^{12}$ genome copy/mL (#AV4808c). $AAV_{2/8}$-CaMKIIα:hM4Di-mCherry was acquired from Addgene with a titer of $2.5*10^{13}$ genome copy/mL (a gift from Bryan Roth, #50477). $AAV_{2/5}$-CaMKIIα:mCherry was acquired from the UNC

Vector Core, with a titer of $3.3*10^{12}$ genome copy/mL (#AV4809D). pAAV-PRAM-d2tTA:TRE-NLS-mKate2 was acquired from Addgene and was serotyped with AAV_9 coat proteins and packaged at the University of Texas Southwestern Medical Center to make $AAV_{2/9}$-PRAM:d2tTA-TRE:NLS-mKate2 with a titer of $9.6*10^{11}$ genome copy/mL (a gift from Yingxi Lin, #84474) (Sorensen et al., 2016). The pAAV-PRAM-d2tTA:TRE-HA-hM4Di was constructed by AgeI-AscI HA-hM4Di fragments (pAAV-CaMKIIα-hM4Di-mCherry: from Addgene plasmid #50477) amplified by PCR using following primers (sense: tcagatcgccaccgggccaccatgtacccatacgatgttccagattacgctgccaacttcaca; antisense: tggatcgctggcgcgctacctggcagtgccgatgt). The resulting fragment was subcloned into the AgeI-AscI sites of pAAV-PRAM-d2tTA:TRE-NLS-mKate2 (a gift from Yingxin Lin, Addgene plasmid #84474) (Sorensen et al., 2016) using the In-Fusion HD Cloning Plus kit (Takara). All constructs were verified by sequencing. Constructs were serotyped with AAV_9 coat proteins and packaged at the University of Texas Southwestern Medical Center to make $AAV_{2/9}$-PRAM:d2tTA-TRE:HA-hM4Di with a titer of $2.8*10^{12}$ genome copy/mL (Konno and Hirai, 2020). $AAV_{2/5}$-CaMKIIα:GCaMP6f was acquired from Addgene with a titer of $2.3*10^{13}$ genome copy/mL (a gift from James M. Wilson, #100834). $AAV_{2/8}$-hSyn:hM4Di-mCherry was acquired from the Addgene, with a titer of $2.0*10^{13}$ genome copy/mL (a gift from Bryan Roth, #50475). $AAV_{2/8}$-hSyn:mCherry was acquired from Addgene, with a titer $2.6*10^{13}$ genome copy/mL (a gift from Karl Deisseroth, #114472).

Stereotaxic Surgeries—All surgeries were conducted using asceptic technique and followed NIH and UT Southwestern IACUC guidelines. A digital small animal stereotax (David Kopf Instruments) with a stereomicroscope (Leica) was used to perform all stereotaxic procedures. Mice were anesthetized with isoflurane (4% for induction, 1–2.5% for maintenance). Microinjections were completed with 10 μL Hamilton microsyringe filled with mineral oil and with a glass micropipette (Drummond Scientific Company) filled with mineral oil attached. A microsyringe pump (World Precision Instruments) was used to control injection speed and volume. The micropipette was slowly lowered to the target site and remained for 5 minutes after injection. Mice were given meloxicam (2 mg/kg) as a post-surgical analgesic, remained on the heating pad until fully recovered from the anesthesia, and were allowed to recover a minimum of three days before returning to group housing with cagemates. To verify target sites, post-mortem histology was performed.

Histology and Immunohistochemistry—Mice were deeply anesthetized with a ketamine (75 mg/kg) / dexmedetomidine (1 mg/kg) cocktail and transcardially perfused with 4% paraformaldehyde (PFA) in PBS. Brains were removed and post-fixed in 4% PFA in PBS at 4°C for 24 hours and then sectioned using a vibratome (Leica) with a thickness of 50 μm. For immunohistochemistry (IHC), tissue sections were incubated in 0.4% Triton-X PBS (PBS-T) with 10% normal goat serum (NGS) for 1 hour. Primary antibodies were then added to PBS-T with 10% NGS and tissue sections were incubated overnight at 4°C. Primary antibodies used for immunostaining were as follows: rabbit anti-Arc (1/500, Synaptic Systems), chicken anti-NeuN (1/1,000, Millipore Sigma), guinea pig anti-NeuN (1/1,000, Millipore Sigma), mouse anti-NeuN (1/1,000, Millipore Sigma), mouse anti-HA (1/1,000, BioLegend), and chicken anti-GFP (1/1000, ThermoFisher Scientific). After rinsing with PBS (3 × 10 min), tissue sections were subsequently incubated with

AlexaFluor405, AlexaFluor488, AlexaFluor546, or AlexaFluor633 conjugated secondary antibodies (1/500, ThermoFisher Scientific) in PBS-T with 10% NGS. Tissue sections were then washed in PBS (3 × 10 min) and mounted in VECTASHIELD medium (Vector Laboratories) on glass slides. Some sections were counterstained with DAPI (1/1,000, ThermoFisher Scientific). Fluorescence images were taken with a Zeiss AxioImager M2 microscope with Apotome using the 2.5x, 5x, and 10x objectives or with Zeiss LSM800 with Airyscan using 10x or 25x objectives. Images were processed using the Zen Blue software.

Roles of ACC and BLA on Exp and Naive OF

Stereotaxic Surgery and Behavior for Optogenetic Inhibition ACC Terminals at BLA—To characterize the necessity of the anterior cingulate cortex (ACC) to basolateral amygdala (BLA) pathway in Naive OF and Exp OF (Figure 2A–H), we bilaterally injected $AAV_{2/5}$-CaMKIIα:eArchT-eYFP (experimental) or $AAV_{2/5}$-CaMKIIα:eYFP (control) in ACC (400 nL/injection, 3.0 nL/sec) aimed at the following coordinates relative to bregma: AP: +2.00 mm, +1.00 mm, and −0.40 mm; ML: ±0.30 mm; DV: −1.50 mm. Next, we bilaterally implanted optical fibers (Doric Lenses) in BLA at the following coordinates relative to bregma: AP: −1.40 mm; ML: ±3.40 mm; DV: −5.00 mm. We used two skull screws and dental cement (C&B Metabond, Parkell) to secure the $_{optical}$ fibers. To further protect the optical fibers, the top part of an Eppendorf tube was attached and secured with dental cement. Mice were allowed to recover for three weeks before returning to group housing with cagemates for one week. For Naive OF on Day 1, observers were bilaterally connected to a 532 nm laser (UltraLasers) controlled by a function generator (Siglent Technologies) and green light stimulation (15 mW, each hemisphere) was illuminated during each electrical shock delivered to the demonstrator. For Naive OF on Day 2, observers were subjected to the same optogenetic protocol except the green light stimulation was illuminated for the demonstrator's shock interval (8 sec light / 10 sec shock interval). For Exp OF, after CFC on Day 1, a similar optogenetic protocol was applied to observers on Day 2 Exp OF (green light stimulation during electrical shock delivery to the demonstrator) and Day 3 Exp OF (green light stimulation 13 sec / 15 sec shock interval).

NMDA-Induced Excitotoxic Lesion of ACC or BLA—To further characterize the necessity of the ACC and BLA in Naive OF and Exp OF, both regions were bilaterally lesioned (Figure S3A–H) in observers by injecting 25 mg/mL N-Methyl-D-aspartic acid (NMDA, Sigma) dissolved in saline. A sham lesion was performed by bilaterally injecting saline only to the target regions. For ACC, injections (150 nL/injection, 3.0 nL/sec) were aimed at the following coordinates relative to bregma: AP: +2.00 mm, +1.00 mm, and −0.10 mm; ML: ±0.30 mm; DV: −1.50 mm. For BLA, injections (150 nL/injection, 3.0 nL/sec) were aimed at the following coordinates relative to bregma: AP: −1.40 mm; ML: ±3.40 mm; DV: −5.00 mm. Observers were allowed to recover for one week before returning to group housing with cagemates. One week after group housing with cagemates, observers were tested for either Naive OF or Exp OF. To verify NMDA-induced excitotoxic lesion of ACC and BLA neurons in both Naive OF and Exp OF groups, 1 coronal section from 3 AP coordinates (ACC; AP; +2.00 mm / +1.00 mm / −0.10 mm, BLA; AP; −1.20 mm / −1.60 mm / −2.00 mm), for a total of 3 coronal sections per mouse, in both experimental

and control groups were immunostained for NeuN. Regions of Interest (ROIs) were selected using the Zen Lite software (Zeiss) around ACC or BLA. The ratio of NeuN channel intensity to background channel intensity was calculated (ROI NeuN channel intensity / section background channel intensity) and compared between experimental and control groups (Figure S3H).

Quantification of Arc Expression in ACC and BLA Neurons during Exp OF and Naive OF—To examine the neural activity in ACC and BLA during Naive OF and Exp OF, we immunostained and quantified expression of the immediate early gene Arc (activity-regulated cytoskeleton-associated protein) (Bramham et al., 2008; Guzowski et al., 1999; Lyford et al., 1995) and the neuronal marker NeuN. We collected 2–4 coronals section from 3 AP coordinates (AP; +2.00 mm / +1.00 mm / −0.10 mm) per mouse for ACC, and 2–4 coronal sections from 3 AP coordinates (AP; −1.20 mm / −1.60 mm / −2.00 mm) per mouse for BLA (Figure 2I–L, S3I). In Figure 2J (ACC), we examined a total of 106,347 (−/−/−: 48,099, S/−/−: 58,248) $NeuN^+$ cells. In Figure 2J (BLA), we examined a total of 38,389 (−/−/−: 17,459, S/−/−: 20,930) $NeuN^+$ cells. In Figure 2L (ACC), we examined a total of 84,034 (−/+/−: 27,860, W/+/+: 56,174) $NeuN^+$ cells. In Figure 2L (BLA), we examined a total of 35,078 (−/+/−: 19,800, W/+/+: 15,278) $NeuN^+$ cells. Quantification of NeuN and Arc positive cells in ACC and BLA was conducted using the Cell Counting plugin in ImageJ. The percentage of Arc^+ neurons in ACC and BLA for each observer in each group was calculated out of total neurons and compared.

In vivo Electrophysiology in ACC and BLA—To further assess ACC, BLA, and vHPC neural activity during Exp OF, multisite electrophysiological recordings were performed using stereotrodes (Figure 2M–O, Figure S4), which were prepared by winding tungsten wires (0.001 inch, 50–150 kΩ, California Fine Wire) similar to the previously reported tetrode fabrication (Osanai et al., 2019). Four sets of stereotrode were mounted on a 3D-printed custom-designed microdrive (3.1 g), which was implanted aimed at the following coordinates relative to bregma for ACC: AP: +1.00 mm; ML: −0.30 mm; DV: 1.50 mm, BLA: AP: −1.40 mm; ML: +3.40 mm; DV: −5.30 mm, and vHPC: AP: −3.18 mm; ML: +3.75 mm; DV: −4.75 mm. White matter served as a reference electrode: AP: −2.40 mm; ML: +2.00 mm; DV: −1.00 mm. The stereotrode tips were coated with Dil (Biotium) to verify correct electrode position (Figure S4A). A stainless steel screw located in the skull lying above the cerebellum served as a ground. Mice were allowed to recover one week after implantation, and were then group housed with their cagemate in a modified cage that contained a perforated divider in the middle, so that the implant could be protected. Local field potentials were band-pass filtered (1 Hz–500 Hz) and acquired with 2 kHz sampling rate using a Neuralynx Digital Lynx 4SX acquisition system. To ensure that we had enough time for adequate LFP data collection, we extended the Exp OF protocol so that there was a 5 minute habituation period and a 6 minute demonstrator shock period (0.5 mA, 2-sec foot shock with a shock interval of 15 seconds for a total of 24 shock trials). After recording sessions were completed, postmortem histology was performed to confirm electrode tip placement. Analysis for electrophysiological data was performed using custom written scripts in MATLAB (MathWorks). A time-varying power of LFP was estimated using Morse’s wavelets (0.07 Hz steps). Power spectral analysis was performed

using the MATLAB pmtm function with 3.0 time-halfbandwidth product, which applies the Thomson's multitaper method (Babadi and Brown, 2014; Thomson, 1982). For the shock period data, each 15-sec time-windowed data were aligned to the stimulation onsets on the demonstrator mice (total 24 trials) and the power spectrums were calculated and averaged for each trial. Similarly, for the habituation period data, 15-sec time-windowed data were segmented from whole habituation period (total 20 segments) and the power spectrums were calculated and averaged for each segment. For calculating cross-correlation between brain areas (Figure 2O), we used the LFP data for whole habituation period (5 min) and shock period (6 min). To verify the quality of the electrophysiological recordings as an internal positive control, we recorded from mice during immobile/sleep (velocity < 0.2 cm/s) and active moving states (velocity > 1.5 cm/s) in a familiar recording box (70 cm W × 45 cm D × 20 cm H) prior to subjecting mice to Exp OF (Figure S4D–F). While we successfully recording during exposure to the familiar recording box from 4 mice, 1 mouse was not used in Figure S4D–F because it did not exhibit enough immobile/sleep state to analyze. We found that the theta/delta power ratio was higher both in ACC and BLA when the mice were actively running than when they were immobile (Figure S4D–E). We also observed a clear peak in the power spectrum at theta range (4–12 Hz) during running compared with the immobile state (Figure S4D–E). These analyses support the reliability of our LFP recording as well as the capability of these recordings to detect the state-dependent LFP changes in ACC and BLA.

Roles of Dorsoventral Hippocampal Activity on Exp and Naive OF

Stereotaxic Surgery for Inhibitory DREADD Experiments—We targeted inhibitory designer receptors exclusively activated by designer drugs (inhibitory DREADDs) to dHPC or vHPC (Roth, 2016). For chemogenetic inhibition of dHPC or vHPC neurons during Exp OF and Naive OF, observers were bilaterally injected with $AAV_{2/8}$-CaMKIIα:hM4Di-mCherry (experimental) or $AAV_{2/5}$-CaMKIIα:mCherry (control). For dHPC, injections (500 nL/injection, 3.0 nL/sec) were aimed at the following coordinates relative to bregma: AP: −2.00 mm; ML: ±1.50 mm; DV: −1.40 mm. For vHPC, injections (500 nL/injection, 3.0 nL/sec) were aimed at the following coordinates relative to bregma: AP: −3.16 mm; ML: ±3.20 mm; DV: −4.70 mm. Mice were allowed to recover for two weeks before returning to group housing with cagemates. One week after group housing with cagemates, mice were tested for behavior. Clozapine N-oxide (CNO, 4 mg/kg, Enzo Life Sciences) was used to activate DREADDs in all behavioral studies.

Behavior Schedule for Inhibitory DREADD Experiments—For DREADD inhibition during CFC on Day 1 in Exp OF, we injected experimental and control observers intraperitoneally (i.p.) with CNO 30 minutes prior to CFC. We then subjected observers to Exp OF on Day 2 (Figure 3G–I). We verified that CNO itself during CFC did not affect observer behavior during Exp OF by injecting non-hM4Di expressing observers i.p. with CNO or saline vehicle 30 minutes prior to CFC on Day 1 (Figure S5C–D). For DREADD inhibition during Exp OF on Day 2 in Exp OF, we first subjected observers to CFC on Day 1. 30 minutes prior to Exp OF on Day 2, we injected experimental and control observers i.p. with CNO (Figure 3J–L). We verified that CNO itself did not affect observer behavior during wOF in a subset of mice by injecting non-hM4Di expressing observers i.p. with CNO

and hM4Di-expressing observers i.p. with saline vehicle 30 minutes prior to Exp OF on Day 2 (Figure S5E–F). For DREADD inhibition during Naive OF, we injected experimental and control observers i.p. with CNO 30 minutes prior to Naive OF (Figure 3M–O).

Ex vivo Electrophysiology to Verify Inhibitory DREADD Efficacy in dHPC and vHPC Neurons—Mice were transcardially perfused with a calcium free sucrose-supplemented cutting solution (in mM; 3 KCl, 4.12 MgSO4, 1.2 NaH2PO4, 206 sucrose, 25 NaHCO3, 25 glucose) chilled to 1–3 °C and suffused with a 5% CO2 balanced-oxygen mix (Airgas). Brains were rapidly removed following perfusion, halved along the sagittal sulcus, and then cut in the either the sagittal plane in 250 μm sections from the ventral lateral surface moving medially for dorsal CA1 recordings, or the horizontal plane moving from the ventral surface to the dorsal in 250 μm sections for ventral CA1 recordings. Cutting was performed on a Leica VT1000 S vibratome. Cutting occurred in oxygenated calcium free sucrose-supplemented cutting solution at 1–3 °C. Slices were then transferred into a 3D printed beaker insert containing a nylon mesh which was submerged in continuously oxygenated extracellular recording solution (in mM; 3 KCl, 1.2 CaCl2, 1.2 MgSO4, 1.2 NaH2PO4, 125 NaCl, 25 NaHCO3, 25 glucose) and maintained at 36°C within a hot water bath for 30 min. The beaker was removed from the bath and allowed to come to room temperature for 30 minutes prior to recording. The slices were continuously maintained at room temperature until used for the recordings.

Slices were continuously perfused with oxygenated extracellular recording solution warmed to 30–34 °C by an in-line heater (Warner Instruments) controlled by an external temperature control unit (Warner Instruments). The CA1 subfield was visualized using a 2.5x objective on a Zeiss Axio Examiner A1 microscope. Magnification was switched to a 63x fluid-immersion objective to visualize individual pyramidal cells within the pyramidal layer. Pipettes for whole cell patch clamp were pulled (Narishige) from borosilicate glass pipettes (World Precision Instruments) to a resistance of 3–7 MΩ. Patch pipettes were filled with intracellular recording solution containing (in mM) 135 KMeSO4, 10 HEPES, 2 MgATP, 0.1 NaGTP, 8 NaCl, 0.1 BAPTAK4, biocytin 0.2% (pH 7.25). Membrane potentials were recorded using a MultiClamp 700B amplifier (Molecular Devices), processed using a Digidata 1550B digitizer. Recordings and analysis used Clampex/Clampfit 11.2 software (Molecular Devices) on a Microsoft Windows-based computer. Membrane potentials were recorded before, during, and after a ramping current injection from 0 to 300 pA over 500 ms, and in response to sequential, step-wise 25 pA current injections from −100 pA to 400 pA, and lasting 500 ms each with 800 ms total between sweeps. In one case, the current ramp failed to induce firing at 300 pA, and the maximum current injection was increased to 500 pA. After baseline recordings were obtained, ongoing passive recording of the membrane potential was engaged while 10 μM CNO (HelloBio) was added to the perfusate. A timestamp was made in the recording when CNO reached the tissue chamber, approximately three minutes after the recording began. The recording was terminated 10 minutes later, and the ramp and current step protocols were repeated. Recordings were acquired with a lowpass filter at 4 kHz, and a sampling rate of 10 kHz at 1x gain.

All electrophysiological data was filtered using the Boxcar method with 5 smoothing points prior to analysis. Rheobase was determined using the current ramp protocol to identify the

current level at which cells began firing (Figure 3C–F). Capacitance was calculated from Tau and Resistance measures acquired with the sweep protocol. Decrease in membrane potential was measured as the change in membrane potential from the timestamp at which the CNO reached the recording chamber and the 8-minute mark from CNO application (Figure 3C–F). Baseline drift was corrected from the slope of the pre-CNO application period.

Quantification of Arc Expression in dHPC CA1 and vHPC CA1 after Exp OF— To examine the neural activity in dCA1 and vCA1 after Exp OF, we immunostained and quantified expression of the immediate early gene Arc and the neuronal marker NeuN. We collected 2–6 coronal sections (AP; −2.00 mm) per mouse for dCA1 and 2–6 coronal sections (AP; −3.16 mm) per mouse for vCA1 (Table S2D). In Table S2D for dCA1, we examined a total of 10,001 (W/−/+: 2,749, W/+/+: 7,252) $NeuN^+$ cells. In Table S2D for vCA1, we examined a total of 21,872 (W/−/+: 10,398, W/+/+: 11,474) $NeuN^+$ cells. Quantification of NeuN and Arc positive cells in ACC and BLA was conducted using the Cell Counting plugin in ImageJ. The percentage of Arc^+ neurons in ACC and BLA for each observer in each group was calculated out of total neurons and compared.

Quantification of Arc Expression in BLA under DREADD Inhibition of dHPC or vHPC—To examine how dHPC and vHPC neural activity regulates BLA neural activity during CFC or Exp OF, we bilaterally targeted inhibitory DREADD (hM4Di) or mCherry as a control to dHPC or vHPC. For DREADD inhibition in dHPC during CFC, we injected observers i.p. with CNO 30 minutes prior to CFC and perfused mice 60 minutes after CFC (Figure 4A–B). For DREADD inhibition in vHPC during Exp OF, we injected observers i.p. with CNO 30 minutes prior to wOF and perfused mice 1 hour after Exp OF (Figure 4C–D). Home cage (HC) control mice were perfused directly from their home cages on the same day. We then immunostained for Arc and NeuN, and compared Arc expression in BLA between homecage, mCherry, and hM4Di groups. We collected 2–4 BLA coronal sections from 3 AP coordinates (AP; −1.20 mm / −1.60 mm / −2.00 mm) per mouse. In Figure 4B, we examined a total of 51,441 (Home cage control: 11,518, mCherry: 17,918, hM4Di: 22,005) $NeuN^+$ cells. In Figure 4D, we examined a total of 57,686 (Home cage control: 14,270, mCherry: 20,207, hM4Di: 23,209) $NeuN^+$ cells. Quantification of NeuN and Arc positive cells in BLA was conducted using the Cell Counting plugin in ImageJ. The percentage of Arc^+ neurons in BLA for each observer in each group was calculated out of total neurons and compared.

We further verified the efficacy of hM4Di DREADD to inhibit dHPC or vHPC by immunostaining mice with dHPC-hM4Di or mCherry and mice with vHPC-hM4Di or mCherry from the above experiments with Arc and NeuN. We then used the ImageJ software to draw ROIs around the cell layer of the dHPC or vHPC CA1 region. The ratio of Arc channel intensity to background channel intensity (arbitrary units, a.u.) was calculated and compared between experimental and control groups for dCA1 (mCherry vs. hM4Di, Figure S5A) and vCA1 (mCherry vs. hM4Di, Figure S5B).

Experience-dependent enhancement of OF using the strong OF protocol—We verified that, regardless of demonstrator shock protocol, observers still exhibit experience-

dependent enhancement of OF and that this experience-dependent enhancement of OF still depends on the vHPC and ACC. Thus, we subjected observers to Exp OF but we used the strong OF protocol during the demonstrator shock period (Exp+sOF, S/+/+, Figure S6, S13).

We compared observer freezing response in the Naive OF protocol with Exp+sOF protocol (Figure S6A–B). 1 hour after behavioral testing, mice were perfused and immunostained for Arc and NeuN. We collected 2–4 vHPC coronal sections (AP; −3.20 mm) per mouse and 2–4 ACC coronal sections from 3 AP coordinates (AP; +2.00 mm / +1.00 mm / −0.10 mm). In Figure S6C for vHPC, we examined 20,057 (Naive OF: 10,864, Exp+sOF: 9,193) $NeuN^+$ cells. In Figure S13C for ACC, we examined 72,962 (Negative control: 21,306, Naive OF: 26,453, Exp+sOF 25,203) $NeuN^+$ cells. Quantification of NeuN and Arc positive cells was conducted using the Cell Counting plugin in ImageJ. The percentage of Arc^+ neurons out of total $NeuN^+$ neurons was calculated and compared between groups (Figure S6C, S13C).

To examine how vHPC neural activity regulates observer freezing response during Exp+sOF, we bilaterally targeted inhibitory DREADD (hM4Di) or mCherry as a control to vHPC (Figure S6D–E). 30 minutes prior to Exp+sOF, mice were injected i.p. with CNO (Figure S6E).

To examine how ACC neural activity regulates observer freezing response during Exp+sOF, we lesioned ACC by injecting NMDA or Saline as a control. (Figure S13A–B).

Role of dHPC and vHPC in Exp OF after auditory fear conditioning—To test whether dHPC and vHPC are necessary for Exp OF regardless of prior shock protocol, we bilaterally injected mice with $AAV_{2/8}$-CaMKIIα:hM4Di-mCherry (experimental) or $AAV_{2/5}$-CaMKIIα:mCherry (control). For dHPC, injections (500 nL/injection, 3.0 nL/sec) were aimed at the following coordinates relative to bregma: AP: −2.00 mm; ML: ±1.50 mm; DV: −1.40 mm. For vHPC, injections (500 nL/injection, 3.0 nL/sec) were aimed at the following coordinates relative to bregma: AP: −3.16 mm; ML: ±3.20 mm; DV: −4.70 mm. Mice were then allowed to recover for two weeks, and were subsequently group housed with cagemates for one week. Mice were then subjected to AFC + Exp OF, with Day 1 AFC and Day 2 Exp OF. For dHPC DREADD-treated observers, we injected observers i.p. with CNO 30 minutes prior to AFC on Day 1 and then tested mice for Exp OF on Day 2 (Figure S10A–C). For vHPC DREADD-treated observers, we subjected observers to AFC on Day 1. On Day 2, we injected observers i.p. with CNO 30 minutes prior to Exp OF and then subjected them to Exp OF (Figure S10D–F).

Immediate shock protocol experiment—To further demonstrate that Exp OF is CFC-dependent and requires enhanced BLA activity on Day 1, we used the immediate shock protocol (Figure S11), which does not produce CFC (Fanselow, 1980; Landeira-Fernandez et al., 2006; Rosen et al., 1998; Wiltgen et al., 2001). We compared OF freezing response in observer mice subjected on Day 1 to context exposure (CTX; exposure to the conditioned context, but no shock, for 3 minutes), to immediate shock (IS; immediate 2-second 0.5 mA shock upon entering the conditioned context and then immediate removal), and to CFC (Figure S11A). In a different cohort, we subjected mice to CTX, IS, or CFC and then perfused the mice 1 hour after testing. We immunostained for Arc and NeuN, and compared

Arc expression in BLA between the CTX, IS, and CFC groups. We collected 2–4 each BLA coronal section from 3 AP coordinates (AP; −1.20 mm / −1.60 mm / −2.00 mm) per mouse. In Figure S11B, we examined a total of 39,699 (CTX group: 15,461, IS group: 11,450, CFC group: 12,788) $NeuN^+$ cells. Quantification of NeuN and Arc positive cells in BLA was conducted using the Cell Counting plugin in ImageJ. The percentage of Arc^+ neurons in BLA for each observer in each group was calculated out of total neurons and compared.

Role of Memory Engram Cells in BLA and Hippocampal CA1 on Exp OF

Stereotaxic Surgery for Engram Reactivation Experiments—To label the subpopulation of BLA, dHPC CA1, ACC, or vHPC CA1 neurons activated during CFC, we conducted doxycycline-off (off-Dox) activity-dependent cell tagging using a Robust Activity Marking (RAM) system (Sorensen et al., 2016; Sun et al., 2020). Observers were bilaterally injected with $AAV_{2/9}$-PRAM:d2tTA-TRE:NLS-mKate2. For BLA, injections (300 nL/injection, 3.0 nL/sec) were aimed at the following coordinates relative to bregma: AP: −1.40 mm; ML: ±3.40 mm; DV: −5.00 mm. For dHPC dCA1, injections (200 nL/injection, 3.0 nL/sec) were aimed at the following coordinates: AP: −2.00 mm relative to bregma; ML: ±1.50 mm relative to bregma; DV: −1.30 mm relative to dura. For ACC, injections (300 nL/injection, 3.0 nL/sec) were aimed at the following coordinates relative to bregma: AP: +1.00 mm; ML: ±0.30 mm; DV: −1.50 mm. For vHPC CA1, injections (300 nL/injection, 3.0 nL/sec) were aimed at the following coordinates relative to bregma: AP: −3.16 mm; ML: ±3.20 mm; DV: −4.70 mm. Mice were allowed to recover for two weeks before returning to group housing with prior cagemates. For all overlapping experiments, mice were maintained on a doxycylene diet (on-Dox, 40 mg/kg, Bio-serv) starting 7 days prior to microinjections.

Behavior and Histology for Engram Reactivation Experiments—Mice were removed from the Dox diet (off-Dox) 48 hours prior to the start of CFC on Day 1. After CFC, mice were immediately put back on the Dox diet. On Day 2, for both BLA-injected and dHPC dCA1-injected mice, a subset of mice were re-exposed to the CFC context and another subset of mice were exposed to Exp OF (Figure 4E–K, S7A). ACC-injected and vCA1-injected mice, after being subjected to CFC on Day 1, were subjected to Exp OF on Day 2 (Table S2A). Additional control groups for BLA CFC/Exp OF mice include the an unrelated aversive experience (Figure 5E–G), a familiar cagemate demonstrator that does not get shocked during wOF (No Demonstrator Shock (−/+/+), Figure 6A, 6D, S7G), an unfamiliar stranger demonstrator that gets shocked during wOF (Stranger Demonstrator (W/+/−), Figure 6A, 6E, S7G), the Switch condition in which OF is conducted on Day 1 and CFC is conducted on Day 2 (Figure S8), and reactivation of the BLA fear memory ensemble labeled on Day 1 CFC on Day 3 Exp OF (after Day 2 Exp OF, Figure S14A–C). 1 hour after the final behavior test, mice were perfused and immunostained for Arc and NeuN. Neurons activated by CFC were labeled with mKate2, and neurons activated by Exp OF were labeled with Arc antibody. We collected 2–4 BLA coronal sections from 3 AP coordinates (AP; −1.20 mm / −1.60 mm / −2.00 mm) per mouse, 3–4 dCA1 coronal sections (AP; 2.00 mm) per mouse, 3–6 ACC coronal sections (AP; +1.00) per mouse, and 3–6 vCA1 coronal sections (AP; −3.16) per mouse. In Figure 4G, we examined a total of 16,880 $NeuN^+$ cells for BLA-injected mice re-exposed to the conditioned context

on Day 2. In Figure 4H, we examined a total of 16,558 $NeuN^+$ cells for BLA-injected mice exposed to Exp OF on Day 2. In Figure 4J, we examined a total of 4,496 $NeuN^+$ cells for dCA1-injected mice re-exposed to the conditioned context on Day 2. In Figure 4K, we examined a total of 5,159 $NeuN^+$ cells for dCA1-injected mice exposed to Exp OF on Day 2. In Table S2A for ACC, we examined a total of 19,167 $NeuN^+$ cells for ACC-injected mice exposed to Exp OF on Day 2. In Table S2A for vHPC CA1, we examined a total of 11,247 $NeuN^+$ cells for vCA1-injected mice exposed to Exp OF on Day 2. In Figure 5G, we examined a total of 13,348 $NeuN^+$ cells for BLA-injected mice in the Light Stress condition. In Figure 6D, we examined a total of 15,916 $NeuN^+$ cells for BLA-injected mice exposed to a familiar cagemate demonstrator that was not shocked on Day 2 (No Demonstrator Shock −/+/+). In Figure 6E, we examined 16,444 $NeuN^+$ cells for BLA-injected mice exposed to an unfamiliar stranger demonstrator that gets shocked during wOF on Day 2 (Stranger Demonstrator W/+/−). In Figure S8D, we examined a total of 17,187 $NeuN^+$ cells for BLA-injected mice in Switch condition exposed to Day 1 OF and Day 2 CFC. In Figure S14D, we examined a total of 10,350 $NeuN^+$ cells for BLA-injected mice tested on Day 3 Exp OF (after Day 1 CFC and Day 2 Exp OF). Quantification of NeuN, Arc, and mKate2 positive cells in ACC and BLA was conducted using the Cell Counting plugin in ImageJ. For $Arc^+mKate2^+$ experiments, the percentages of Arc positive $mKate2^-$ and $mKate2^+$ neurons in each group was calculated and compared for all groups. Chance level of overlap index was calculated per mouse with the following formula: $(\frac{Total\ Arc\ positive\ cells}{Total\ NeuN\ positive\ cells} * \frac{Total\ mKate2 positive\ cells}{Total\ NeuN\ positive\ cells} * 100\%)$. Chance level of overlap index was then compared with actual percent overlap of $Arc^+mKate2^+$ neurons $(\frac{Arc+mKate2+cells}{Total\ NeuN\ positive\ cells} * 100\%)$ for all groups. Fold change analysis $(\frac{Actual\ percent\ overlap\ of\ Arc+mKate2+cells}{Chance\ percent\ overlap\ of\ Arc+mKate2+cells} * 100\%)$ was calculated and compared (Figure S7F–G, S14C).

Inhibition of BLA Engram Cells During CFC Context Re-exposure or Exp OF—Mice were maintained on a Dox diet starting 7 days prior to microinjections. Stereotaxic procedures for this experiment were the same as the BLA engram reactivation experiments, except experimental mice were injected with $AAV_{2/9}$-PRAM-d2tTA:TRE-HA-hM4Di, whereas control mice were injected with $AAV_{2/9}$-PRAM:d2tTA:TRE-NLS-mKate2. Mice were removed from the Dox diet 48 hours prior to the start of CFC on Day 1 (Figure 5A). After CFC, mice were immediately put back on the Dox diet. On Day 2, mice were injected i.p. with CNO and, 30 minutes later, were either re-exposed to the CFC context or tested for Exp OF (Figure 5C–D).

To verify the efficacy of HA-hM4Di to inhibit the activation of the BLA neurons formed during CFC on Day 1 during Exp OF on Day 2, a subset of BLA $AAV_{2/9}$-PRAM:d2tTA-TRE:HA-hM4Di observers or BLA $AAV_{2/9}$-PRAM:d2tTA-TRE:NLS-mKate2 observers were perfused 1 hour after Exp OF and immunostained for Arc and NeuN. We collected 2 BLA coronal sections (AP; −1.60 mm) per mouse. In Figure S6D–E, we examined a total of 8,455 (mKate2: 3,731, HA-hM4Di: 4,724) $NeuN^+$ cells. Quantification of NeuN, Arc, HA, and mKate2 positive cells in BLA was conducted using the Cell Counting plugin in ImageJ. Chance and Actual overlap of Arc^+HA^+ neurons and $Arc^+mKate2^+$ neurons, the

percentages of Arc positive HA^- and HA^+ neurons, and the percentages of Arc positive $mKate2^-$ and $mKate2^+$ neurons was calculated and compared (Figure S6D–E), as described above.

Inhibition of a BLA Neural Ensemble Labeled by an Unrelated Aversive Experience During Exp OF—Mice were maintained on a Dox diet starting 7 days prior to microinjections. Stereotaxic procedures for this experiment were the same as the BLA engram cell inhibition experiment described in the previous section. Mice were maintained on-Dox for 3 weeks and then subjected to CFC. 24 hours after CFC training, mice were removed from the Dox diet for 2 days. Mice were then subjected to an unrelated aversive experience (bright light exposure on an elevated platform). Mice were placed on top of an elevated platform (92 cm tall, 91 cm diameter) with a bright overhead light (about 1,900 lux) for 10 minutes. After the bright light exposure on an elevated platform, mice were immediately put back on-Dox. The next day, mice were injected i.p. with CNO and then, 30 minutes later, were tested for Exp OF (Figure 5E).

vHPC Regulation of the Reactivation of BLA Engram Cells During Exp OF —To examine how vHPC regulates the reactivation of the BLA engram cells encoding CFC memory during Exp OF, we bilaterally targeted inhibitory DREADD ($AAV_{2/8}$-CaMKIIα:hM4Di-mCherry) or mCherry control ($AAV_{2/5}$-CaMKIIα:mCherry) to vHPC (coordinates relative to bregma: AP: −3.16 mm; ML: ±3.20 mm; DV: −4.70 mm) and bilaterally targeted $AAV_{2/9}$-PRAM:d2tTA-TRE:NLS-mKate2 to BLA (coordinates relative to bregma: AP: −1.40 mm; ML: ±3.40 mm; DV: −5.00 mm). Mice were removed from the Dox diet 48 hours prior to the start of CFC on Day 1. After CFC, mice were immediately put back on the Dox diet. On Day 2, mice were injected i.p. with CNO and, 30 minutes later, were tested for Exp OF. 1 hour after Exp OF, mice were perfused and immunostained for Arc and NeuN (Figure 6A–C, S7F). We collected 2–4 each BLA coronal section from 3 AP coordinates (AP; −1.20 mm / −1.60 mm / −2.00 mm) per mouse. In Figure 6B, we examined a total of 12,420 $NeuN^+$ cells for vHPC-injected mCherry mice (Exp OF / mCherry in vHPC), In Figure 6C, we examined a total of 11,492 $NeuN^+$ cells for vHPC-injected hM4Di-mCherry mice (Exp OF / hM4Di in vHPC). Quantification of NeuN, Arc, and mKate2 positive cells in BLA was conducted using the Cell Counting plugin in ImageJ. Chance and Actual overlap of $Arc^+mKate2^+$ neurons, the percentages of Arc positive $mKate2^-$ and $mKate2^+$ neurons, and fold change analysis was calculated and compared (Figure 6B–C, S7A), as described above.

in vivo Calcium Imaging in BLA and vHPC

Stereotaxic Surgery—For *in vivo* calcium imaging from BLA, unilateral viral injection (500 nL, 100 nL/min) of $AAV_{2/5}$-CaMKIIα:GCaMP6f, a calcium indicator (Chen et al., 2013), was aimed at the BLA at the following coordinates relative to bregma: AP: −1.40 mm; ML: +3.40 mm; DV: −5.00 mm. Mice were allowed to recover for 1 week before being group-housed with their cagemate. 3 weeks after AAV injection, a micro gradient-index (GRIN) lens (0.60 mm diameter, 7.30 mm length, Inscopix) was implanted targeting the BLA after aspiration with a blunt 27-gauge needle with the following coordinates relative to bregma (center of needle or lens): AP: −1.40 mm; ML: +3.40 mm; DV: 4.50 mm

(aspiration), −4.80 mm (lens implantation). The lens was held in place by several skull screws and dental cement (C&B Metabond, Parkell). Mice were allowed to recover for 10–14 days. For *in vivo* calcium imaging from vHPC, unilateral viral injection (500 nL/3 DV coordinates, 100 nL/min) of $AAV_{2/5}$-CaMKIIα:GCaMP6f was aimed at the vHPC at the following coordinates relative to bregma: AP: −3.16; ML: +3.25 mm; DV: −4.70, −4.35, and −4.10 mm. Mice were allowed to recover for 1 week before being group housed with their cagemate. 3 weeks after AAV injection, the tissue was cut with a #11 scalpel blade to prepare for microprism GRIN lens insertion at the following coordinates relative to bregma (measured from the tip of the blade): AP: − 2.60 mm through −3.60 mm; ML: +4.25 mm; DV: −4.25 mm. Immediately after cutting the tissue, a microprism GRIN lens (1.00 mm diameter, 9.10 mm length, Inscopix) was implanted targeting the vHPC with the following coordinates relative to bregma: AP: −3.10 mm (center of medial side of lens); ML: +4.25 mm initial insertion, +4.05 mm final placement (medial side of lens); DV: −4.25 mm (posterior ventral tip of medial side of lens). The lens was held in place by several skull screws and dental cement (C&B Metabond, Parkell). Mice were allowed to recover for 10–14 days. 10–14 days after lens implantation to BLA or vHPC, the baseplate (Inscopix) for the miniature microscope camera was attached above the lens using a UV-cured glue (Norland). 3 days after baseplate attachment, mice were group housed with their cagemate in a modified cage that contained a perforated divider in the middle, so that the implant could be protected. Mice were group housed with their cagemate for 1 week prior to the start of imaging experiments, and were habituated to the camera during that week.

Behavior and Image Capturing—Implanted mice underwent calcium imaging during the Exp OF. For the BLA imaging experiment (Figure 5H–K, S9), mice were imaged during CFC on Day 1 and were imaged during Exp OF with a cagemate demonstrator on Day 2. For vHPC imaging experiment (Figure 6F–I), mice were subjected to CFC on Day 1 (but not imaged). Mice were then imaged during Exp OF with a familiar cagemate demonstrator on Day 2, and then imaged during Exp OF with an unfamiliar stranger demonstrator on Day 3. During imaging, calcium activity was captured at 20 Hz using a miniature fluorescent microscope (Inscopix). Recording sessions were triggered with a sustained TTL signal to allow for simultaneous acquisition of calcium activity and observer behavior.

Image Processing and Analysis—We examined somatic calcium activity ($\Delta F/F$) of individual neurons from BLA or vHPC. To analyze movie files collected over multiple days, we used the Inscopix Mosaic Software v1.2.0 to concatenate movie files for each mouse before beginning image processing. We used the Inscopix Data Processing Software v1.2.1 with default settings to pre-process, spatial bandpass filter (low cut-off = 0.005 $pixel^{-1}$, high cut-off = 0.500 $pixel^{-1}$), and motion correct concatenated movie files. Next, we used the Inscopix Mosaic Software to spatially downsample processed movie files by a factor of 2 and temporally downsample processed movie files by a factor of 4. Processed movies were then imported into ImageJ and ROIs (~1/4 cell body size at center of the cell body) were carefully drawn around putative cells for each day of imaging. Individual cells were visually tracked based on the cell location and shape in the stacked images, as previously demonstrated (Kitamura et al., 2017; Okuyama et al., 2016; Roy et al., 2017; Zhang et al., 2020). ROIs were carefully examined if they represented a putative cell on day 1 of imaging,

day 2 of imaging, or both days of imaging. The ImageJ software was used to acquire *ΔF/F* activity for each ROI for each frame of processed movie files.

For the following calculations, the moving average (n = 5) for the *ΔF/F* values was calculated for each ROI for each frame. Next, each ROI was checked for significant calcium events, which we defined as (local maximum > 3*SD(*ΔF/F)* + Mean(*ΔF/F*)) for a given imaging session. ROIs that did not have any significant calcium events were excluded from analysis. We classified cells as "Shock Responding (SR) Cells" (defined as a significant increase in average *ΔF/F* intensity in response to own shock or demonstrator's shock during the demonstrator shock period), "Shock Suppressed (SS) Cells" (defined as a significant decrease in average *ΔF/F* intensity in response to own shock or demonstrator's shock during the demonstrator shock period), and "Non-Shock Responding (NSR) Cells" (defined as no change in average *ΔF/F* intensity in response to own or demonstrator's shock during the demonstrator shock period). For BLA, we compared the moving average of *ΔF/F* intensity for SR and Other (SS + NSR) cells during Day 1 CFC and SR, SS, NSR cells during Day 2 Exp OF. We also considered how CFC SR, CFC Other, and all CFC cells during Day 1 CFC respond during Day 2 Exp OF. For vHPC, we compared the moving average of *ΔF/F* intensity between Day 2 Exp OF with a cagemate demonstrator and Day 3 OF with a stranger demonstrator for SR Cells or Other cells. We also considered if the overall proportion of SR/Other cells changes between Day 2 Exp OF with a cagemate demonstrator and Day 3 OF with a stranger demonstrator. Finally, we calculated the Chance vs. Actual overlap for Cagemate/Stranger SR cells. Graphpad Prism 9 software was used for all statistical comparisons.

Role of BLA-Projecting vHPC Neuron Activity on Exp OF

Quantification of Arc expression in BLA-projecting vHPC Neurons during Exp OF—

To examine the neural activity of BLA-projecting vHPC neurons during Exp OF, we bilaterally injected Cholrea Toxin Subunit B (CTB) conjugated to AlexFluor-555 (200 nL per side, 100 nL / min, ThermoFisher Scientific) in BLA aimed at the following coordinates relative to bregma: AP: −1.40 mm; ML: ±3.40 mm; DV: −5.00 mm. Mice were allowed to recover for 3 days before returning to group housing with cagemates. On Day 1, observers were subjected to CFC. On Day 2, we then tested observers for Exp OF with a familiar demonstrator (W/+/+) or with stranger demonstrator (W/+/−). 1 hour after behavioral testing, mice were perfused and immunostained for Arc and NeuN. We collected 2–4 vHPC coronal sections (AP; −3.20 mm) per mouse. In Figure 7B, we examined a total of 12,872 (W/+/−: 5,943, W/+/+: 6,929) $NeuN^+$ cells. The percentage of total Arc^+CTB^+ neurons was calculated out of total CTB^+ cells ($\frac{Total\ Arc+CTB+cells}{Total\ CTB+cells} * 100\%$). Fold change analysis (normalized by the average of the control W/+/− group) was compared between groups. The percentage of total Arc^+CTB^- neurons was calculated out of total CTB^- cells ($\frac{Total\ Arc+CTB-cells}{Total\ CTB-cells} * 100\%$). Fold change analysis (normalized by the average of the control W/+/− group) was compared between groups. Quantification of NeuN, CTB, and Arc positive cells in vHPC was conducted using the Cell Counting plugin in ImageJ.

Stereotaxic Surgery and Behavior for Optogenetic Inhibition of vHPC Terminals at BLA—To identify the functional vHPC-BLA excitatory neurons to Exp OF during the demonstrator's shock moments (Figure 7C–D), we bilaterally injected $AAV_{2/5}$-CaMKIIα:eArchT-eYFP (experimental) or $AAV_{2/5}$-CaMKIIα:eYFP (control) in vHPC (500 nL/injection, 3.0 nL/sec) aimed at the following coordinates relative to bregma: AP: −3.16 mm; ML: ±3.20 mm; DV: −4.70 mm. Next, we bilaterally implanted optical fibers (Doric Lenses) in BLA at the following coordinates relative to bregma: AP: −1.40 mm; ML: ±3.40 mm; DV: −5.00 mm. We used two skull screws and dental cement (C&B Metabond, Parkell) to secure the optical fibers. To further protect the optical fibers, the top part of an Eppendorf tube was attached and secured with dental cement. Mice were allowed to recover for three weeks before returning to group housing with cagemates. On Day 1, observers were subjected to CFC. On Day 2, the optical fiber implants were bilaterally connected to a 532 nm laser (UltraLasers) controlled by a function generator (Siglent Technologies) and green light stimulation (15 mW, each hemisphere) was illuminated during each electrical shock delivered to the demonstrator (Figure 7C–D).

Effect of Optogenetic Terminal Inhibition of vHPC neurons at BLA on the Reactivation of BLA Fear Memory Engram Cells—Mice were maintained on a Dox diet starting 7 days prior to surgical treatment (Figure 7E). To determine whether BLA-projecting vHPC excitatory neurons access the BLA fear memory engram cells during the demonstrator's shock moments in Exp OF, mice were bilaterally injected $AAV_{2/5}$-CaMKIIα:eArchT-eYFP (experimental) or $AAV_{2/5}$-CaMKIIα:eYFP (control) in vHPC (500 nL/injection, 3.0 nL/sec) aimed at the following coordinates relative to bregma: AP: −3.16 mm; ML: ±3.20 mm; DV: −4.70 mm. Next, we bilaterally injected BLA (300 nL/injection, 3.0 nL/sec) with $AAV_{2/9}$-PRAM:d2tTA-TRE:NLS-mKate2 aimed at the following coordinates relative to bregma: AP: −1.40 mm; ML: ±3.40 mm; DV: −5.00 mm. Then, we bilaterally implanted optical fibers in BLA at the following coordinates relative to bregma: AP: −1.40 mm; ML: ±3.40 mm; DV: −5.00 mm and secured the optical fibers as described in the section above. Mice were allowed to recover for three weeks before returning to group housing with cagemates. Mice were removed from the Dox diet 48 hours prior to the start of CFC on Day 1. After CFC, mice were immediately put back on the Dox diet. On Day 2, fiber implants were bilaterally connected to a 532 nm laser (UltraLasers), with the settings of the laser described in the section above. Green light stimulation was illuminated during each electrical shock delivery to the demonstrator. 1 hour after Exp OF, mice were perfused and immunostained for Arc and NeuN. Neurons activated by CFC were labeled with mKate2, and neurons activated by Exp OF were labeled with Arc antibody. We collected 2–4 each BLA coronal sections from 3 AP coordinates (AP; −1.20 mm / −1.60 mm / −2.00 mm) per mouse. In Figure 7E–K, we examined a total of 33,711 (eYFP group: 16,165, eArchT group: 17,546) $NeuN^+$ cells. Quantification of NeuN, Arc, and mKate2 positive cells in BLA was conducted using the Cell Counting plugin in ImageJ. The percentages of Arc positive $mKate2^-$ and $mKate2^+$ neurons, chance and actual overlap of $Arc^+mKate2^+$ neurons, and fold change analysis was calculated and compared (Figure 7G–H, 7K), as described above. We compared Arc^+ neurons in $mKate2^+$ neurons and Arc^+ neurons in $mKate2^-$ neurons between eYFP and eArchT groups (Figure 7I–J).

Stereotaxic Surgery and Behavior Schedule for DREADD Inhibition of Medial Prefrontal Cortex and Nucleus Accumbens—For chemogenetic inhibition of the medial prefrontal cortex (mPFC) or nucleus accumbens (NAc) neurons during Exp OF, observers were bilaterally injected with $AAV_{2/8}$-CaMKIIα:hM4Di-mCherry (experimental) or $AAV_{2/5}$-CaMKIIα:mCherry (control) in mPFC, or bilaterally injected with $AAV_{2/8}$-hSyn:hM4Di-mCherry (experimental) or $AAV_{2/8}$-hSyn:mCherry (control) in NAc. For mPFC injections (300 nL/injection, 3.0 nL/sec) were aimed at the following coordinates relative to bregma: AP: +2.00 mm; ML: ±0.30 mm; DV: −2.00 mm. For NAc, injections (300 nL/injection, 3.0 nL/sec) were aimed at the following coordinates relative to bregma: AP: +1.50 mm; ML: ±0.60 mm; DV: −4.70 mm. Mice were allowed to recover for two weeks before returning to group housing with cagemates. One week after group housing with cagemates, mice were tested for Exp OF. Observers were first subjected to CFC on Day 1. 30 minutes prior to Exp OF on Day 2, we injected experimental and control observers i.p. with CNO (Figure S12A–F).

Quantification of Arc Expression in Amygdala subregions after Exp OF.—To examine the role of different amygdala subregions in Exp OF, we quantified neural activity in the BLA, lateral amygdala (LA), central amygdala (CeA), and basomedial amygdala (BMA) with Arc. We collected 2–4 coronal sections (AP; −1.20 mm / −1.60 mm / −2.00 mm) per mouse (Figure S12G–H). In S12H for BLA, we examined a total of 11,145 (W/−/+: 4,544, W/+/+: 6,901) $NeuN^+$ cells. In S12H for LA, we examined a total of 4,207 (W/−/+: 2,373, W/+/+: 1,834) $NeuN^+$ cells. In S12H for CeA, we examined a total of 3,786 (W/−/+: 2,049, W/+/+: 1,737) $NeuN^+$ cells. In S12H for BMA, we examined a total of 5,584 (W/−/+: 2,926, W/+/+: 2,658) $NeuN^+$ cells. Quantification of NeuN and Arc positive cells in BLA, LA, CeA, and BMA was conducted using the Cell Counting plugin in ImageJ. The percentage of Arc^+ neurons in ACC and BLA for each observer in each group was calculated out of total neurons and compared.

Inhibition of the NMDA Receptor Activation in Exp OF—To examine the role of synaptic plasticity in Exp OF, we inhibited the NMDA receptor activation with CPP, a selective and competitive antagonist of NMDA receptors (Figure S14D–E) (Hrabetova and Charlton Sacktor, 1997; Rodríguez et al., 2005; Suzuki et al., 2004). On Day 1, mice were subject to CFC. 30 minutes prior to Exp OF on Day 2, mice were given i.p. injection of CPP (10 mg / kg) or saline vehicle as a control (Figure S14E).

Quantification and Statistical Analysis

Data are presented as mean values accompanied by the Standard Error of the Mean (SEM), except for box plots, which are presented as the minimum, first quartile, median, third quartile, and maximum. Statistical methods were not used to predetermine sample sizes in experiments; sample sizes were based on what is conventional for the field and previous literature (Jeon et al., 2010; Kitamura et al., 2017; Okuyama et al., 2016). Mice were randomly assigned to groups. Comparisons were between subjects or measured repeatedly as noted in the text. Experimenters were blinded to the conditions of experiments during data analysis. Graphpad Prism 9 software was used for statistical analyses. One-way ANOVA with the Tukey-Kramer test, one-way repeated measures ANOVA with the

Tukey-Kramer test, two-way mixed ANOVA, unpaired t-tested (two-sided), paired t-test (two-sided), one sample t-test, Mann-Whitney U-test (two-sided), and chi-square test were used when appropriate. The null hypothesis was rejected at the $P < 0.05$ level. All statistical values including ANOVAs, F values, t values, and additional statistical information are presented in supplemental figures and supplementary table.

Supplementary Material

Refer to Web version on PubMed Central for supplementary material.

Acknowledgements

We thank all members of the Kitamura laboratory for their support, Dr. Shari Birnbaum for advice on behavioral approaches, and Drs. Brad Pfeiffer and Daisuke Hattori for their comments on the manuscript. This work was supported by grants from Endowed Scholar Program to T.K, Brain Research Foundation to T.K (BRFSG-2018-04), Faculty Science and Technology Acquisition and Retention Program to T.K, the Brain & Behavior Research Foundation to T.K (26391), J.Yo (28801), the Whitehall Foundation to T.K (2019-05-38), National Institute of Mental Health to T.K (R01MH120134, R01MH125916), J.T (F32MH119721) and W.M (T32MH076690, F32MH122082), National Institute on Drug Abuse to J.T (T32DA007290), Daiichi Sankyo Foundation of Life Science to J.Yo, Uehara Memorial Foundation to J.Yo, and Japan Society for the Promotion of Science to H.O (201860198).

References

Adolphs R (2013). The Biology of Fear. Current Biology 23, R79–R93. [PubMed: 23347946]

Allsop SA, Wichmann R, Mills F, Burgos-Robles A, Chang C-J, Felix-Ortiz AC, Vienne A, Beyeler A, Izadmehr EM, Glober G, et al. (2018). Corticoamygdala Transfer of Socially Derived Information Gates Observational Learning. Cell 173, 1329–1342.e1318. [PubMed: 29731170]

Andersen SM, and Chen S (2002). The relational self: An interpersonal social-cognitive theory. Psychological Review 109, 619–645. [PubMed: 12374322]

Aron A, Norman CC, and Aron EN (1998). The self-expansion model and motivation. Representative Research in Social Psychology 22, 1–13.

Aron EN, and Aron A (1996). Love and expansion of the self: The state of the model. Personal Relationships 3, 45–58.

Atsak P, Orre M, Bakker P, Cerliani L, Roozendaal B, Gazzola V, Moita M, and Keysers C (2011). Experience modulates vicarious freezing in rats: a model for empathy. PLoS One 6, e21855. [PubMed: 21765921]

Babadi B, and Brown EN (2014). A Review of Multitaper Spectral Analysis. IEEE Transactions on Biomedical Engineering 61, 1555–1564. [PubMed: 24759284]

Barrett LF, Mesquita B, Ochsner KN, and Gross JJ (2007). The Experience of Emotion. Annual Review of Psychology 58, 373–403.

Bazelot M, Bocchio M, Kasugai Y, Fischer D, Dodson PD, Ferraguti F, and Capogna M (2015). Hippocampal Theta Input to the Amygdala Shapes Feedforward Inhibition to Gate Heterosynaptic Plasticity. Neuron 87, 1290–1303. [PubMed: 26402610]

Beckes L, Coan JA, and Hasselmo K (2013). Familiarity promotes the blurring of self and other in the neural representation of threat. Soc Cogn Affect Neurosci 8, 670–677. [PubMed: 22563005]

Ben-Ami Bartal I, Decety J, and Mason P (2011). Empathy and pro-social behavior in rats. Science 334, 1427–1430. [PubMed: 22158823]

Bramham CR, Worley PF, Moore MJ, and Guzowski JF (2008). The immediate early gene arc/arg3.1: regulation, mechanisms, and function. J Neurosci 28, 11760–11767. [PubMed: 19005037]

Burgos-Robles A, Gothard KM, Monfils MH, Morozov A, and Vicentic A (2019). Conserved features of anterior cingulate networks support observational learning across species. Neurosci Biobehav Rev 107, 215–228. [PubMed: 31509768]

Burkett JP, Andari E, Johnson ZV, Curry DC, de Waal FB, and Young LJ (2016). Oxytocin-dependent consolation behavior in rodents. Science 351, 375–378. [PubMed: 26798013]

Cai DJ, Aharoni D, Shuman T, Shobe J, Biane J, Song W, Wei B, Veshkini M, La-Vu M, Lou J, et al. (2016). A shared neural ensemble links distinct contextual memories encoded close in time. Nature 534, 115–118. [PubMed: 27251287]

Cao Y, Contreras-Huerta LS, McFadyen J, and Cunnington R (2015). Racial bias in neural response to others' pain is reduced with other-race contact. Cortex 70, 68–78. [PubMed: 25798570]

Carrillo M, Han Y, Migliorati F, Liu M, Gazzola V, and Keysers C (2019). Emotional Mirror Neurons in the Rat's Anterior Cingulate Cortex. Curr Biol 29, 1301–1312 e1306. [PubMed: 30982647]

Cheetham SA, Thom MD, Jury F, Ollier WE, Beynon RJ, and Hurst JL (2007). The genetic basis of individual-recognition signals in the mouse. Curr Biol 17, 1771–1777. [PubMed: 17949982]

Chen Q, Panksepp JB, and Lahvis GP (2009). Empathy is moderated by genetic background in mice. PLoS One 4, e4387. [PubMed: 19209221]

Chen TW, Wardill TJ, Sun Y, Pulver SR, Renninger SL, Baohan A, Schreiter ER, Kerr RA, Orger MB, Jayaraman V, et al. (2013). Ultrasensitive fluorescent proteins for imaging neuronal activity. Nature 499, 295–300. [PubMed: 23868258]

Choi J, and Jeong Y (2017). Elevated emotional contagion in a mouse model of Alzheimer's disease is associated with increased synchronization in the insula and amygdala. Sci Rep 7, 46262. [PubMed: 28387348]

Choi JH, Sim SE, Kim JI, Choi DI, Oh J, Ye S, Lee J, Kim T, Ko HG, Lim CS, et al. (2018). Interregional synaptic maps among engram cells underlie memory formation. Science 360, 430–435. [PubMed: 29700265]

Church RM (1959). Emotional reactions of rats to the pain of others. J Comp Physiol Psychol 52, 132–134. [PubMed: 13654562]

Ciocchi S, Passecker J, Malagon-Vina H, Mikus N, and Klausberger T (2015). Selective information routing by ventral hippocampal CA1 projection neurons. Science 348, 560–563. [PubMed: 25931556]

Corder G, Ahanonu B, Grewe BF, Wang D, Schnitzer MJ, and Scherrer G (2019). An amygdalar neural ensemble that encodes the unpleasantness of pain. Science 363, 276–281. [PubMed: 30655440]

Cruz A, Heinemans M, Marquez C, and Moita MA (2020). Freezing Displayed by Others Is a Learned Cue of Danger Resulting from Co-experiencing Own Freezing and Shock. Curr Biol 30, 1128–1135 e1126. [PubMed: 32032509]

Debiec J, and Olsson A (2017). Social Fear Learning: from Animal Models to Human Function. Trends Cogn Sci 21, 546–555. [PubMed: 28545935]

Deng X, Gu L, Sui N, Guo J, and Liang J (2019). Parvalbumin interneuron in the ventral hippocampus functions as a discriminator in social memory. Proc Natl Acad Sci U S A 116, 16583–16592. [PubMed: 31358646]

Fanselow MS (1980). Conditioned and unconditional components of post-shock freezing. Pavlov J Biol Sci 15, 177–182. [PubMed: 7208128]

Frankland PW, Ding HK, Takahashi E, Suzuki A, Kida S, and Silva AJ (2006). Stability of recent and remote contextual fear memory. Learn Mem 13, 451–457. [PubMed: 16882861]

Friard O, and Gamba M (2016). BORIS: a free, versatile open-source event-logging software for video/audio coding and live observations. Methods in Ecology and Evolution 7, 1325–1330.

Gallese V, and Goldman A (1998). Mirror neurons and the simulation theory of mind-reading. Trends Cogn Sci 2, 493–501. [PubMed: 21227300]

Gangopadhyay N, and Schilbach L (2012). Seeing minds: A neurophilosophical investigation of the role of perception-action coupling in social perception. Social Neuroscience 7, 410–423. [PubMed: 22059802]

Gibson JJ (1958). Visually Controlled Locomotion and Visual Orientation in Animals. British Journal of Psychology 49, 182–194. [PubMed: 13572790]

Gibson JJ (1979). The ecological approach to visual perception (Boston, MA, US: Houghton, Mifflin and Company).

Golkar A, Castro V, and Olsson A (2015). Social learning of fear and safety is determined by the demonstrator's racial group. Biol Lett 11, 20140817. [PubMed: 25631229]

Gonzalez-Liencres C, Juckel G, Tas C, Friebe A, and Brune M (2014). Emotional contagion in mice: the role of familiarity. Behav Brain Res 263, 16–21. [PubMed: 24480421]

Gordon RM (1986). Folk psychology as simulation. Mind & language 1, 158–171.

Graham J, D'Ambra AF, Jung SJ, Teratani-Ota Y, Vishwakarma N, Venkatesh R, Parigi A, Antzoulatos EG, Fioravante D, and Wiltgen BJ (2021). High-Frequency Stimulation of Ventral CA1 Neurons Reduces Amygdala Activity and Inhibits Fear. Front Behav Neurosci 15, 595049. [PubMed: 33767614]

Guzowski JF, McNaughton BL, Barnes CA, and Worley PF (1999). Environment-specific expression of the immediate-early gene Arc in hippocampal neuronal ensembles. Nat Neurosci 2, 1120–1124. [PubMed: 10570490]

Han Y, Bruls R, Soyman E, Thomas RM, Pentaraki V, Jelinek N, Heinemans M, Bassez I, Verschooren S, Pruis I, et al. (2019). Bidirectional cingulate-dependent danger information transfer across rats. PLoS Biol 17, e3000524. [PubMed: 31805039]

Heal J (1986). Replication and functionalism. In Language, Mind, and Logic, Butterfield J, ed. (Cambridge University Press), pp. 135–150.

Hernandez-Lallement J, Attah AT, Soyman E, Pinhal CM, Gazzola V, and Keysers C (2020). Harm to Others Acts as a Negative Reinforcer in Rats. Curr Biol 30, 949–961 e947. [PubMed: 32142701]

Hong EH, and Choi JS (2018). Observational threat conditioning is induced by circa-strike activity burst but not freezing and requires visual attention. Behav Brain Res 353, 161–167. [PubMed: 30016738]

Hooker CI, Verosky SC, Miyakawa A, Knight RT, and D'Esposito M (2008). The influence of personality on neural mechanisms of observational fear and reward learning. Neuropsychologia 46, 2709–2724. [PubMed: 18573512]

Hrabetova S, and Charlton Sacktor T (1997). Long-term potentiation and long-term depression are induced through pharmacologically distinct NMDA receptors1Portions of this work were previously published in abstract form [11].1. Neuroscience Letters 226, 107–110. [PubMed: 9159501]

Hübner C, Bosch D, Gall A, Lüthi A, and Ehrlich I (2014). Ex vivo dissection of optogenetically activated mPFC and hippocampal inputs to neurons in the basolateral amygdala: implications for fear and emotional memory. Front Behav Neurosci 8, 64. [PubMed: 24634648]

Hunsaker MR, and Kesner RP (2008). Dissociations across the dorsal-ventral axis of CA3 and CA1 for encoding and retrieval of contextual and auditory-cued fear. Neurobiol Learn Mem 89, 61–69. [PubMed: 17931914]

Hurst JL, Payne CE, Nevison CM, Marie AD, Humphries RE, Robertson DH, Cavaggioni A, and Beynon RJ (2001). Individual recognition in mice mediated by major urinary proteins. Nature 414, 631–634. [PubMed: 11740558]

Ito W, Erisir A, and Morozov A (2015). Observation of Distressed Conspecific as a Model of Emotional Trauma Generates Silent Synapses in the Prefrontal-Amygdala Pathway and Enhances Fear Learning, but Ketamine Abolishes those Effects. Neuropsychopharmacology 40, 2536–2545. [PubMed: 25865929]

Ito W, and Morozov A (2019). Prefrontal-amygdala plasticity enabled by observational fear. Neuropsychopharmacology 44, 1778–1787. [PubMed: 30759453]

Jeon D, Kim S, Chetana M, Jo D, Ruley HE, Lin SY, Rabah D, Kinet JP, and Shin HS (2010). Observational fear learning involves affective pain system and Cav1.2 Ca2+ channels in ACC. Nat Neurosci 13, 482–488. [PubMed: 20190743]

Jeon D, and Shin HS (2011). A mouse model for observational fear learning and the empathetic response. Curr Protoc Neurosci Chapter 8, Unit 8 27.

Jimenez JC, Berry JE, Lim SC, Ong SK, Kheirbek MA, and Hen R (2020). Contextual fear memory retrieval by correlated ensembles of ventral CA1 neurons. Nat Commun 11, 3492. [PubMed: 32661319]

John ER, Chesler P, Bartlett F, and Victor I (1968). Observation Learning in Cats. Science 159, 1489–1491. [PubMed: 5732493]

Josselyn SA, and Tonegawa S (2020). Memory engrams: Recalling the past and imagining the future. Science 367.

Kandel ER, Dudai Y, and Mayford MR (2014). The molecular and systems biology of memory. Cell 157, 163–186. [PubMed: 24679534]

Keum S, Kim A, Shin JJ, Kim JH, Park J, and Shin HS (2018). A Missense Variant at the Nrxn3 Locus Enhances Empathy Fear in the Mouse. Neuron 98, 588–601 e585. [PubMed: 29681532]

Keum S, and Shin H-S (2019). Neural Basis of Observational Fear Learning: A Potential Model of Affective Empathy. Neuron 104, 78–86. [PubMed: 31600517]

Kheirbek MA, Drew LJ, Burghardt NS, Costantini DO, Tannenholz L, Ahmari SE, Zeng H, Fenton AA, and Hen R (2013). Differential control of learning and anxiety along the dorsoventral axis of the dentate gyrus. Neuron 77, 955–968. [PubMed: 23473324]

Kim A, Keum S, and Shin HS (2019). Observational fear behavior in rodents as a model for empathy. Genes Brain Behav 18, e12521. [PubMed: 30264490]

Kim BS, Lee J, Bang M, Seo BA, Khalid A, Jung MW, and Jeon D (2014). Differential regulation of observational fear and neural oscillations by serotonin and dopamine in the mouse anterior cingulate cortex. Psychopharmacology (Berl) 231, 4371–4381. [PubMed: 24752658]

Kim EJ, Kim ES, Covey E, and Kim JJ (2010). Social transmission of fear in rats: the role of 22-kHz ultrasonic distress vocalization. PLoS One 5, e15077. [PubMed: 21152023]

Kim JJ, Rison RA, and Fanselow MS (1993). Effects of amygdala, hippocampus, and periaqueductal gray lesions on short- and long-term contextual fear. Behav Neurosci 107, 1093–1098. [PubMed: 8136063]

Kim S-W, Kim M, and Shin H-S (2021). Affective empathy and prosocial behavior in rodents. Current Opinion in Neurobiology 68, 181–189. [PubMed: 34091136]

Kim S, Matyas F, Lee S, Acsady L, and Shin HS (2012). Lateralization of observational fear learning at the cortical but not thalamic level in mice. Proc Natl Acad Sci U S A 109, 15497–15501. [PubMed: 22949656]

Kim WB, and Cho JH (2017). Synaptic Targeting of Double-Projecting Ventral CA1 Hippocampal Neurons to the Medial Prefrontal Cortex and Basal Amygdala. J Neurosci 37, 4868–4882. [PubMed: 28385873]

Kim WB, and Cho JH (2020). Encoding of contextual fear memory in hippocampal-amygdala circuit. Nat Commun 11, 1382. [PubMed: 32170133]

Kitamura T, Ogawa SK, Roy DS, Okuyama T, Morrissey MD, Smith LM, Redondo RL, and Tonegawa S (2017). Engrams and circuits crucial for systems consolidation of a memory. Science 356, 73–78. [PubMed: 28386011]

Kitamura T, Pignatelli M, Suh J, Kohara K, Yoshiki A, Abe K, and Tonegawa S (2014). Island cells control temporal association memory. Science 343, 896–901. [PubMed: 24457215]

Kitamura T, Saitoh Y, Takashima N, Murayama A, Niibori Y, Ageta H, Sekiguchi M, Sugiyama H, and Inokuchi K (2009). Adult neurogenesis modulates the hippocampus-dependent period of associative fear memory. Cell 139, 814–827. [PubMed: 19914173]

Kitamura T, Sun C, Martin J, Kitch LJ, Schnitzer MJ, and Tonegawa S (2015). Entorhinal Cortical Ocean Cells Encode Specific Contexts and Drive Context-Specific Fear Memory. Neuron 87, 1317–1331. [PubMed: 26402611]

Konno A, and Hirai H (2020). Efficient whole brain transduction by systemic infusion of minimally purified AAV-PHP.eB. J Neurosci Methods 346, 108914. [PubMed: 32810474]

Landeira-Fernandez J, DeCola JP, Kim JJ, and Fanselow MS (2006). Immediate shock deficit in fear conditioning: effects of shock manipulations. Behav Neurosci 120, 873–879. [PubMed: 16893293]

LeDoux J (2012). Rethinking the emotional brain. Neuron 73, 653–676. [PubMed: 22365542]

Lidhar NK, Insel N, Dong JY, and Takehara-Nishiuchi K (2017). Observational fear learning in degus is correlated with temporal vocalization patterns. Behav Brain Res 332, 362–371. [PubMed: 28627387]

Liu L, Ito W, and Morozov A (2017). GABAb Receptor Mediates Opposing Adaptations of GABA Release From Two Types of Prefrontal Interneurons After Observational Fear. Neuropsychopharmacology 42, 1272–1283. [PubMed: 27924875]

Liu X, Ramirez S, Pang PT, Puryear CB, Govindarajan A, Deisseroth K, and Tonegawa S (2012). Optogenetic stimulation of a hippocampal engram activates fear memory recall. Nature 484, 381–385. [PubMed: 22441246]

Lyford GL, Yamagata K, Kaufmann WE, Barnes CA, Sanders LK, Copeland NG, Gilbert DJ, Jenkins NA, Lanahan AA, and Worley PF (1995). Arc, a growth factor and activity-regulated gene, encodes a novel cytoskeleton-associated protein that is enriched in neuronal dendrites. Neuron 14, 433–445. [PubMed: 7857651]

Maren S, and Fanselow MS (1997). Electrolytic lesions of the fimbria/fornix, dorsal hippocampus, or entorhinal cortex produce anterograde deficits in contextual fear conditioning in rats. Neurobiol Learn Mem 67, 142–149. [PubMed: 9075242]

Mineka S, Davidson M, Cook M, and Keir R (1984). Observational conditioning of snake fear in rhesus monkeys. J Abnorm Psychol 93, 355–372. [PubMed: 6542574]

Monfils MH, and Agee LA (2019). Insights from social transmission of information in rodents. Genes Brain Behav 18, e12534. [PubMed: 30375171]

Morelli SA, Rameson LT, and Lieberman MD (2014). The neural components of empathy: predicting daily prosocial behavior. Soc Cogn Affect Neurosci 9, 39–47. [PubMed: 22887480]

Okuyama T, Kitamura T, Roy DS, Itohara S, and Tonegawa S (2016). Ventral CA1 neurons store social memory. Science 353, 1536–1541. [PubMed: 27708103]

Olsson A, and Phelps EA (2007). Social learning of fear. Nat Neurosci 10, 1095–1102. [PubMed: 17726475]

Osanai H, Kitamura T, and Yamamoto J (2019). Hybrid Microdrive System with Recoverable Opto-Silicon Probe and Tetrode for Dual-Site High Density Recording in Freely Moving Mice. J Vis Exp.

Panksepp JB, and Lahvis GP (2011). Rodent empathy and affective neuroscience. Neurosci Biobehav Rev 35, 1864–1875. [PubMed: 21672550]

Pellman BA, and Kim JJ (2016). What Can Ethobehavioral Studies Tell Us about the Brain's Fear System? Trends Neurosci 39, 420–431. [PubMed: 27130660]

Pereira AG, Cruz A, Lima SQ, and Moita MA (2012). Silence resulting from the cessation of movement signals danger. Curr Biol 22, R627–628. [PubMed: 22917506]

Pisansky MT, Hanson LR, Gottesman II, and Gewirtz JC (2017). Oxytocin enhances observational fear in mice. Nat Commun 8, 2102. [PubMed: 29235461]

Redondo RL, Kim J, Arons AL, Ramirez S, Liu X, and Tonegawa S (2014). Bidirectional switch of the valence associated with a hippocampal contextual memory engram. Nature 513, 426–430. [PubMed: 25162525]

Roberts SA, Prescott MC, Davidson AJ, McLean L, Beynon RJ, and Hurst JL (2018). Individual odour signatures that mice learn are shaped by involatile major urinary proteins (MUPs). BMC Biol 16, 48. [PubMed: 29703213]

Rodríguez JJ, Davies HA, Silva AT, De Souza IE, Peddie CJ, Colyer FM, Lancashire CL, Fine A, Errington ML, Bliss TV, et al. (2005). Long-term potentiation in the rat dentate gyrus is associated with enhanced Arc/Arg3.1 protein expression in spines, dendrites and glia. Eur J Neurosci 21, 2384–2396. [PubMed: 15932597]

Rosen JB, Fanselow MS, Young SL, Sitcoske M, and Maren S (1998). Immediate-early gene expression in the amygdala following footshock stress and contextual fear conditioning. Brain Res 796, 132–142. [PubMed: 9689463]

Roth BL (2016). DREADDs for Neuroscientists. Neuron 89, 683–694. [PubMed: 26889809]

Roy DS, Kitamura T, Okuyama T, Ogawa SK, Sun C, Obata Y, Yoshiki A, and Tonegawa S (2017). Distinct Neural Circuits for the Formation and Retrieval of Episodic Memories. Cell 170, 1000–1012 e1019. [PubMed: 28823555]

Roy DS, Park Y-G, Ogawa SK, Cho JH, Choi H, Kamensky L, Martin J, Chung K, and Tonegawa S (2019). Brain-wide mapping of contextual fear memory engram ensembles supports the dispersed engram complex hypothesis. bioRxiv, 668483.

Sakaguchi T, Iwasaki S, Okada M, Okamoto K, and Ikegaya Y (2018). Ethanol facilitates socially evoked memory recall in mice by recruiting pain-sensitive anterior cingulate cortical neurons. Nat Commun 9, 3526. [PubMed: 30166546]

Sanders J, Mayford M, and Jeste D (2013). Empathic fear responses in mice are triggered by recognition of a shared experience. PLoS One 8, e74609. [PubMed: 24058601]

Sato N, Tan L, Tate K, and Okada M (2015). Rats demonstrate helping behavior toward a soaked conspecific. Anim Cogn 18, 1039–1047. [PubMed: 25964095]

Silva AJ, Zhou Y, Rogerson T, Shobe J, and Balaji J (2009). Molecular and cellular approaches to memory allocation in neural circuits. Science 326, 391–395. [PubMed: 19833959]

Singer T, Seymour B, O'Doherty J, Kaube H, Dolan RJ, and Frith CD (2004). Empathy for pain involves the affective but not sensory components of pain. Science 303, 1157–1162. [PubMed: 14976305]

Smith ML, Asada N, and Malenka RC (2021). Anterior cingulate inputs to nucleus accumbens control the social transfer of pain and analgesia. Science 371, 153–159. [PubMed: 33414216]

Sorensen AT, Cooper YA, Baratta MV, Weng FJ, Zhang Y, Ramamoorthi K, Fropf R, LaVerriere E, Xue J, Young A, et al. (2016). A robust activity marking system for exploring active neuronal ensembles. Elife 5.

Sun X, Bernstein MJ, Meng M, Rao S, Sorensen AT, Yao L, Zhang X, Anikeeva PO, and Lin Y (2020). Functionally Distinct Neuronal Ensembles within the Memory Engram. Cell 181, 410–423 e417. [PubMed: 32187527]

Suzuki A, Josselyn SA, Frankland PW, Masushige S, Silva AJ, and Kida S (2004). Memory Reconsolidation and Extinction Have Distinct Temporal and Biochemical Signatures. The Journal of Neuroscience 24, 4787–4795. [PubMed: 15152039]

Tanaka KZ, He H, Tomar A, Niisato K, Huang AJY, and McHugh TJ (2018). The hippocampal engram maps experience but not place. Science 361, 392–397. [PubMed: 30049878]

Thomson DJ (1982). Spectrum estimation and harmonic analysis. Proceedings of the IEEE 70, 1055–1096.

Tonegawa S, Liu X, Ramirez S, and Redondo R (2015). Memory Engram Cells Have Come of Age. Neuron 87, 918–931. [PubMed: 26335640]

Tonegawa S, Morrissey MD, and Kitamura T (2018). The role of engram cells in the systems consolidation of memory. Nat Rev Neurosci 19, 485–498. [PubMed: 29970909]

Twining RC, Vantrease JE, Love S, Padival M, and Rosenkranz JA (2017). An intra-amygdala circuit specifically regulates social fear learning. Nat Neurosci 20, 459–469. [PubMed: 28114293]

Wiltgen BJ, Sanders MJ, Anagnostaras SG, Sage JR, and Fanselow MS (2006). Context fear learning in the absence of the hippocampus. J Neurosci 26, 5484–5491. [PubMed: 16707800]

Wiltgen BJ, Sanders MJ, Behne NS, and Fanselow MS (2001). Sex differences, context preexposure, and the immediate shock deficit in Pavlovian context conditioning with mice. Behav Neurosci 115, 26–32. [PubMed: 11256449]

Zhang X, Kim J, and Tonegawa S (2020). Amygdala Reward Neurons Form and Store Fear Extinction Memory. Neuron 105, 1077–1093 e1077. [PubMed: 31952856]

Highlights

1. Hippocampus and amygdala mediate experience-dependent observational fear (Exp OF).
2. Exp OF requires fear memory engram cells encoding prior similar fear experience.
3. Dorsal hippocampus generates memory engram cells in basolateral amygdala (BLA).
4. Ventral hippocampus reactivates memory engram cells in BLA to facilitate Exp OF.

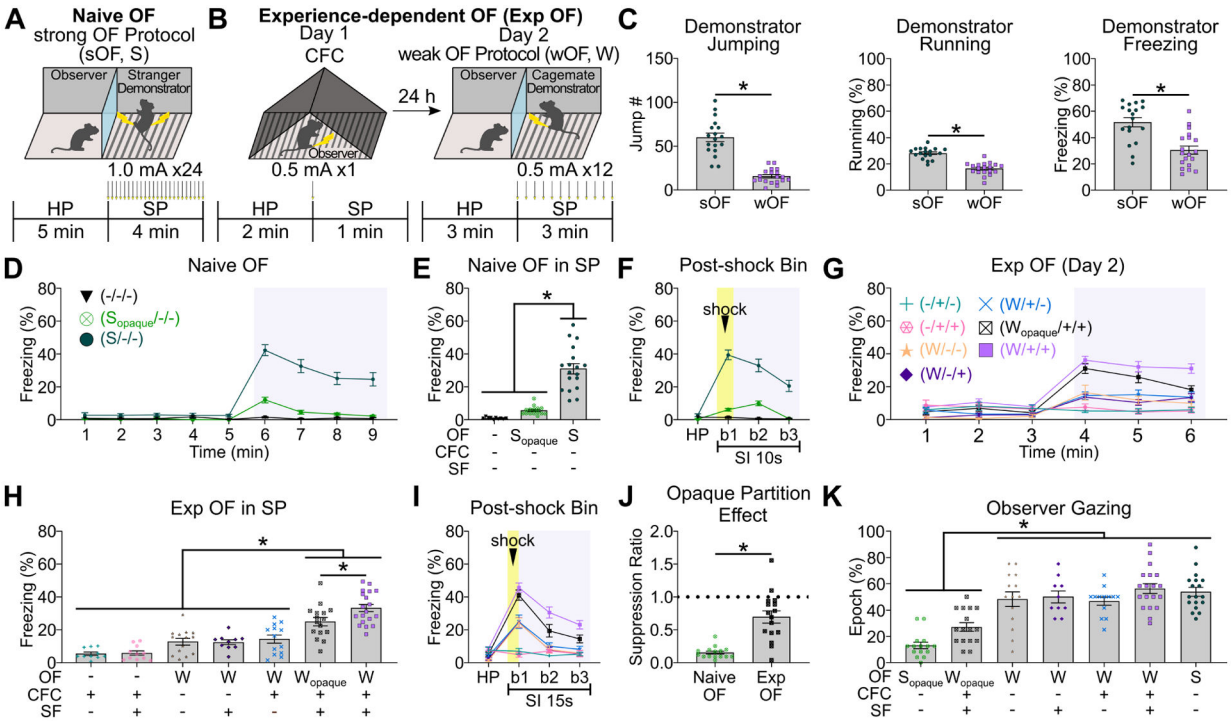

Figure 1: Naive OF and Exp OF behavioral models

(A) Naive Observational Fear (OF) with strong OF protocol (sOF/S). Arrows; electrical shock delivery. HP; habituation period, SP; shock period. **(B)** Experience-Dependent OF (Exp OF) with Day 1 CFC to observer and Day 2 weak OF protocol to demonstrator (wOF/W). CFC; contextual fear conditioning. **(C)** Demonstrator behavior in SP of Naive OF (sOF) and Exp OF (wOF). **(D)** Observer freezing levels in HP (1–5 min) and SP (6–9 min; gray box) of Naive OF or control conditions in 1 min time bins. **(E)** Observer freezing levels in SP of Naive OF. SF; social familiarity. **(F)** Observer freezing levels in post-shock bins in Naive OF. Yellow box; shock delivery to demonstrator (0 sec – 2 sec). Gray box; shock period. SI; shock interval. **(G)** Observer freezing levels in HP (1–3 min) and SP (4–6 min; gray box) of Exp OF or control conditions in 1 min time bins. **(H)** Observer freezing levels in SP of Exp OF. **(I)** Observer freezing levels in post-shock bins in Exp OF. Yellow box; shock delivery to demonstrator (0 sec – 2 sec). Gray box; shock period. **(J)** Suppression ratio of observer freezing by opaque partition. **(K)** Percentages of observer gazing epochs to demonstrator in SP of Exp OF, Naive OF, and the control conditions. Graphs show means ± SEM. * $P < 0.05$ by Mann-Whitney U-test (C, J), two-sided unpaired t-test (C), and one-way ANOVA with Tukey-Kramer test (E, H, K).

In this and in all subsequent figures, bars without asterisks did not reach significance ($P > 0.05$). ANOVAs, F values, t values, and all additional statistical information for this and subsequent figures can be found in the Supplemental Table 1. See also Figure S1–2.

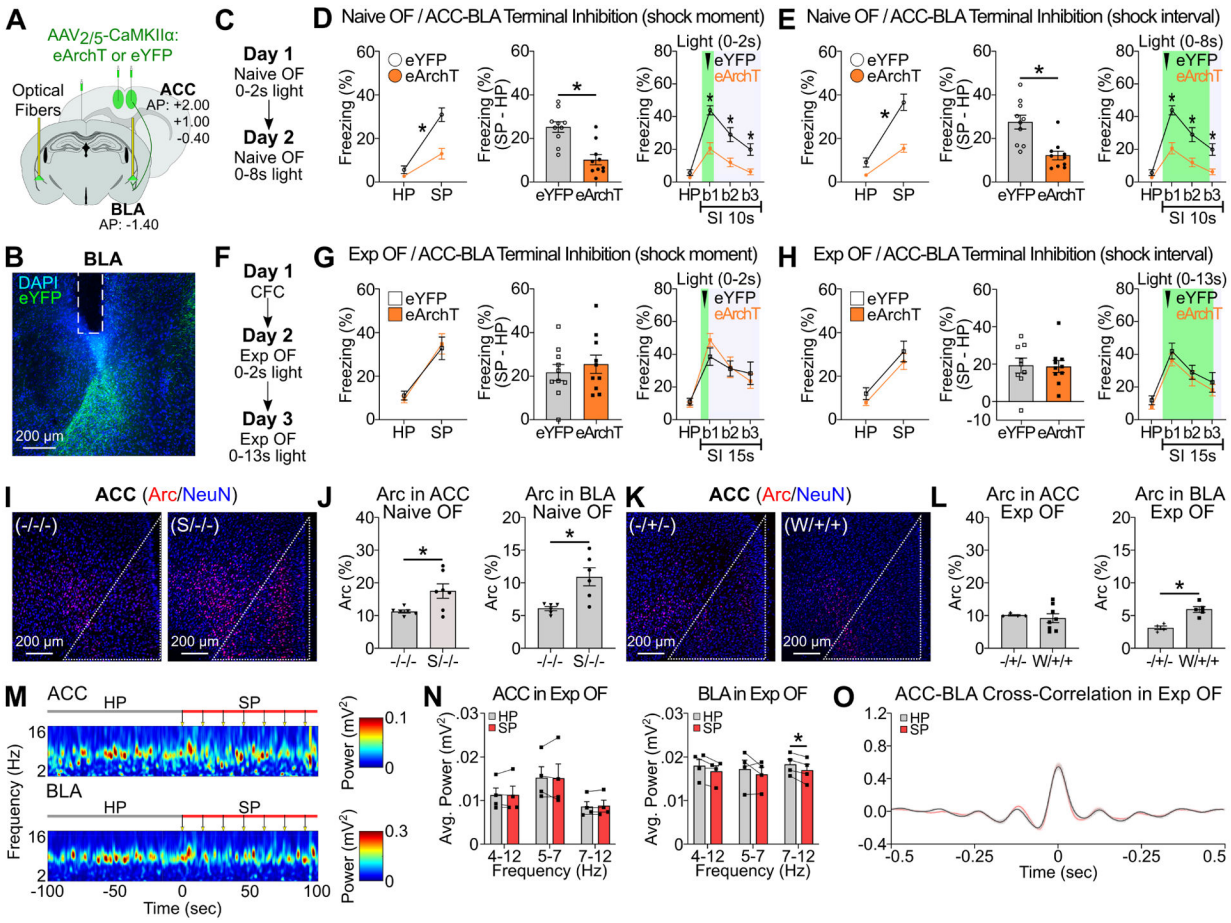

Figure 2: ACC and BLA in Exp OF and Naive OF

(A) Strategy for optogenetic terminal inhibition of ACC neurons at BLA. **(B)** Coronal section of BLA with fiber implantation (white lines) in BLA. **(C, F)** Schedule for Naive OF (C) and Exp OF (F). **(D-E, G-H)** Observer freezing response with optogenetic inhibition of ACC terminals at BLA in Naive OF (D-E) and Exp OF (G-H) during shock moment (D, G) or shock moment+ post shock period (E, H). (Left) Observer freezing levels during HP and SP of eYFP and eArchT groups. (Middle) Subtraction freezing levels (SP–HP) of eYFP and eArchT groups. (Right) Observer freezing levels in post-shock bins. **(I, K)** Coronal sections of Arc/NeuN immunohistochemistry in ACC in Naive OF (I) or Exp OF (K). White lines; ACC region. **(J, L)** Percentages of Arc^{+} neurons in ACC or BLA in Naive OF (J) or Exp OF (L). **(M)** Representative spectrograms of local field potentials (LFPs) in ACC and BLA during HP and SP in Exp OF. Arrows; 2-sec 0.5 mA shock delivered to the demonstrator. **(N)** Averaged theta 4–12 Hz, 5–7 Hz and 7–12 Hz power for ACC (left) and BLA (right) during the HP and SP in Exp OF. **(O)** Averaged cross-correlation of ACC-BLA neural activity during the HP and SP in Exp OF. N = 4 mice. Graphs show means ± SEM. * $P < 0.05$ by interaction with two-way mixed ANOVA (D-E, G-H), two-sided unpaired t-test (D-E, G-H, L), Mann-Whitney U-test (D-E, J, L), and two-sided paired t-test (N-O). See also Supplemental Table 1 and Figure S3–4.

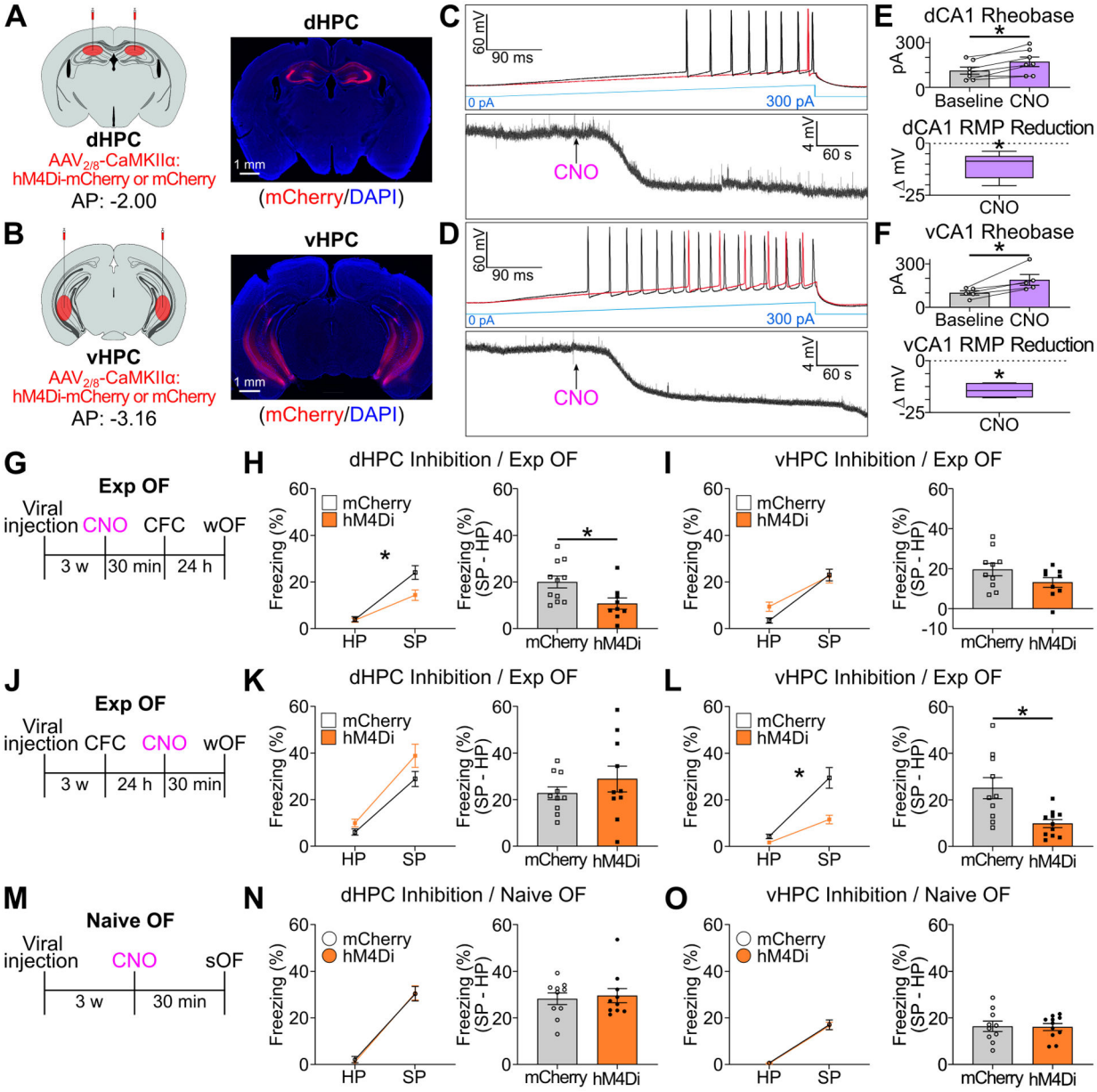

Figure 3. Dorsoventral hippocampus in Exp OF and Naive OF.

(A-B) (Left) Strategy. (Right) Coronal sections of hM4Di-mCherry expression in dHPC (A) or vHPC (B). **(C-D)** Ramping current injection (top) and changes in resting membrane potential (RMP, bottom) in hM4Di$^+$ dCA1 neurons (C) or vCA1 neurons (D) after CNO application. **(E-F)** (Top) Required current injection to evoke action potential before and during CNO application for dHPC-hM4Di (E) and vHPC-hM4Di (F). (Bottom) Change in RMP from baseline in hM4Di$^+$ neurons after CNO application in dCA1 (E) or vCA1 (F). **(G)** Schedule for chemogenetic inhibition of dHPC (H) or vHPC (I) during CFC in Exp OF. **(H-I)** (Left) Observer freezing levels during HP and SP of mCherry and hM4Di groups. (Right) Subtraction freezing levels (SP–HP). **(J)** Schedule for chemogenetic inhibition of dHPC (K) or vHPC (L) during wOF in Exp OF. **(K-L)** (Left) Observer freezing levels

during HP and SP. (Right) Subtraction freezing levels. **(M)** Schedule for chemogenetic inhibition of dHPC (N) or vHPC (O) during sOF in Naive OF. **(N-O)** (Left) Observer freezing levels during HP and SP. (Right) Subtraction freezing levels. Graphs show means ± SEM, except E-F RMP graphs, which are presented as box plots. * $P < 0.05$ by two-sided paired t-test (E-F), one-sample t-test (E-F), interaction with two-way mixed ANOVA (H-I, K-L, N-O), two-sided unpaired t-test (H-I, N-O), and Mann-Whitney U-test (K-L). See also Supplemental Table 1 and Figure S5–6.

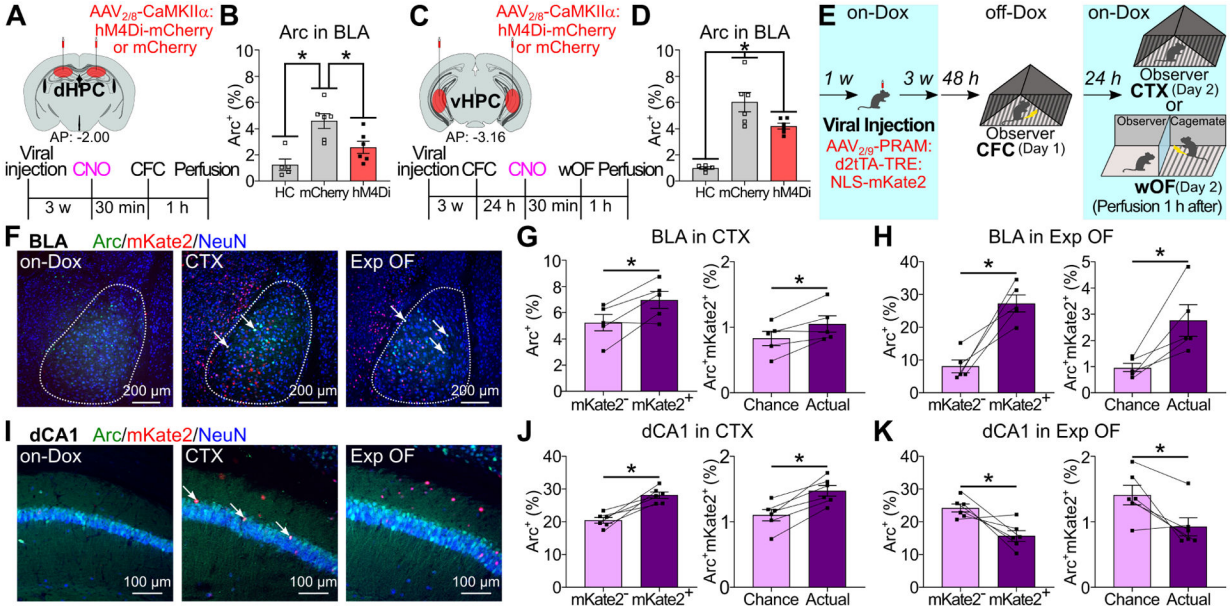

Figure 4. BLA and dHPC CA1 memory engram ensembles in Exp OF.

(A, C) Experimental schedules. **(B, D)** Percentages of Arc^+ neurons in BLA after CFC (B) or Exp OF (D). **(E)** Reactivation of CFC-activated neurons during exposure to conditioned context (CTX) or Exp OF. **(F, I)** Coronal sections of BLA (F) and dCA1 (I) in on-Dox, CTX, and Exp OF. Arrows; $Arc^+mKate2^+$ neurons. **(G-H, J-K)** (Left) Percentages of Arc^+ neurons in $mKate2^-$ and $mKate2^+$ neurons in BLA/CTX, BLA/Exp OF, dCA1/CTX, and dCA1/Exp OF groups. (Right) Actual percentages and chance levels of $Arc^+mKate2^+$ neurons in BLA/CTX, BLA/Exp OF, dCA1/CTX, and dCA1/Exp OF groups. Graphs show means ± SEM. * $P < 0.05$ by one-way ANOVA with Tukey-Kramer test (B, D), and two-sided paired t-test (G-H, J-K). See also Supplemental Table 1 and Figure S7–8.

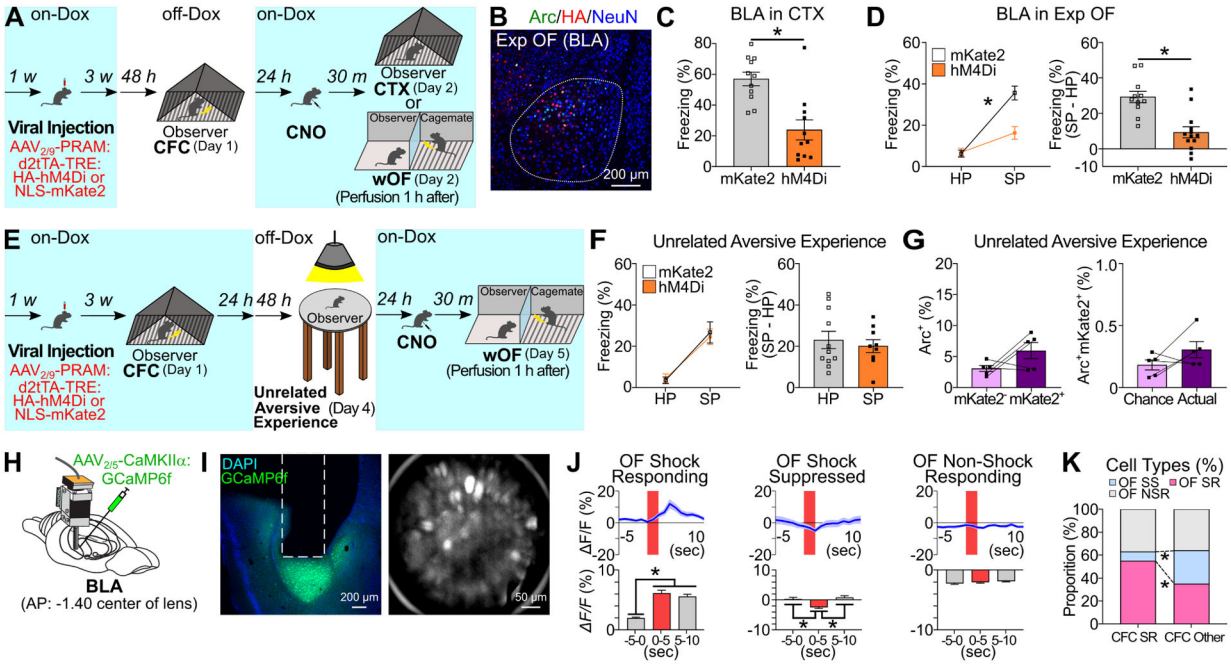

Figure 5. BLA fear memory engram cells in Exp OF.

(A) Inhibition of CFC-activated BLA neurons during CTX (C) or Exp OF (D). **(B)** Coronal section of BLA in Exp OF. **(C)** Freezing levels during CTX in mKate2 and hM4Di groups. **(D)** (Left) Observer freezing levels during HP and SP of mKate2 and hM4Di groups. (Right) Subtraction freezing levels. **(E)** Experimental schedule for inhibition (F) and reactivation (G) of BLA neurons activated by an unrelated aversive experience (bright light exposure on elevated platform) during Exp OF. **(F)** (Left) Observer freezing levels during HP and SP of mKate2 and hM4Di groups. (Right) Subtraction freezing levels. **(G)** (Left) Percentages of Arc^+ neurons in $mKate2^-$ and $mKate2^+$ neurons in BLA during Exp OF. (Right) Actual percentages and chance levels of $Arc^+mKate2^+$ neurons in BLA during Exp OF. **(H)** BLA GRIN lens implantation. **(I)** (Left) Coronal section of BLA in GRIN lens (white lines) implantation. (Right) Stacked image acquired through microendoscope. **(J)** (Top) Averaged calcium activity (*ΔF/F*%) in OF Shock-Responding (SR), Shock-Suppressed (SS), and Non-Shock Responding (NSR) cell during Exp OF. Shock delivery period (red; 2 sec). (Bottom) Averaged calcium activity in −5–0 sec, 0–5 sec, and 5–10 sec period during Exp OF. **(K)** Proportion of OF SR, SS, and NSR cells between CFC SR and Other cells. N = 160 cells. Graphs show means ± SEM. * $P < 0.05$ by two-sided unpaired t-test (C, D, F), interaction with two-way mixed ANOVA (D, F), two-sided paired t-test (G), one-way repeated measures ANOVA with Tukey-Kramer test (J), and chi-square test (K). See also Supplemental Table 1 and Figure S9.

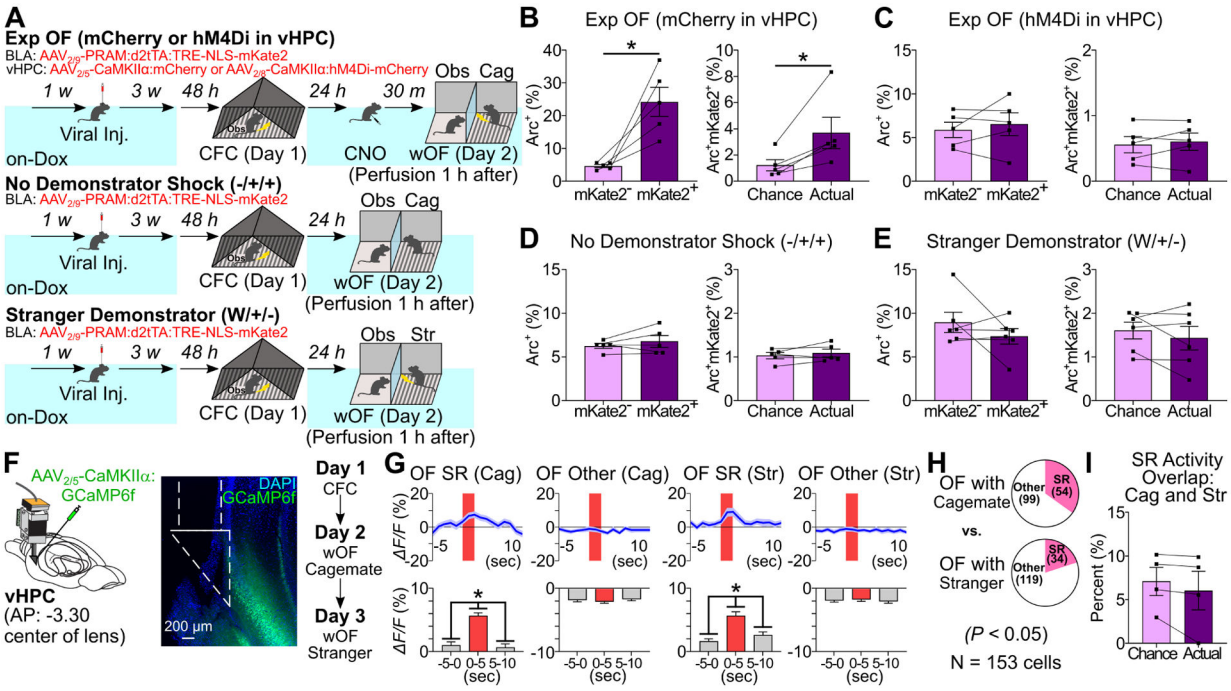

Figure 6. Dynamics and necessity of vHPC neuron activity in Exp OF.

(A) Experimental schedules. **(B-E)** (Left) Percentages of Arc^{+} neurons in mKate2^{-} and mKate2^{+} BLA neurons in Exp OF/mCherry in vHPC, Exp OF/hM4Di in vHPC, No Demonstrator Shock, and Stranger Demonstrator groups. (Right) Actual percentages and chance levels of Arc^{+}mKate2^{+} BLA neurons in Exp OF/mCherry in vHPC, Exp OF/hM4Di in vHPC, No Demonstrator Shock, and Stranger Demonstrator groups. **(F)** (Left) vHPC GRIN lens implantation. (Center) Coronal section of vHPC in GRIN lens (white lines) implantation. (Right) Schedule (imaging on Day 2 and Day 3). **(G)** (Top) Averaged calcium activity (*ΔF/F*%) of Cagemate and Stranger OF SR and OF Other cells during Exp OF. (Bottom) Averaged calcium activity in −5–0 sec, 0–5 sec, and 5–10 sec period during Exp OF. **(H)** Proportion of vHPC OF-SR and OF-Other cells between cagemate and stranger demonstrator. **(I)** Actual percentages and chance levels of Cagemate SR/Stranger SR cells during OF. Graphs show means ± SEM. * P < 0.05 by two-sided paired t-test (B-E, I), one-way repeated measures ANOVA with Tukey-Kramer test (G), and chi-square test (H). See also Supplemental Table 1 and Figure S10–11.

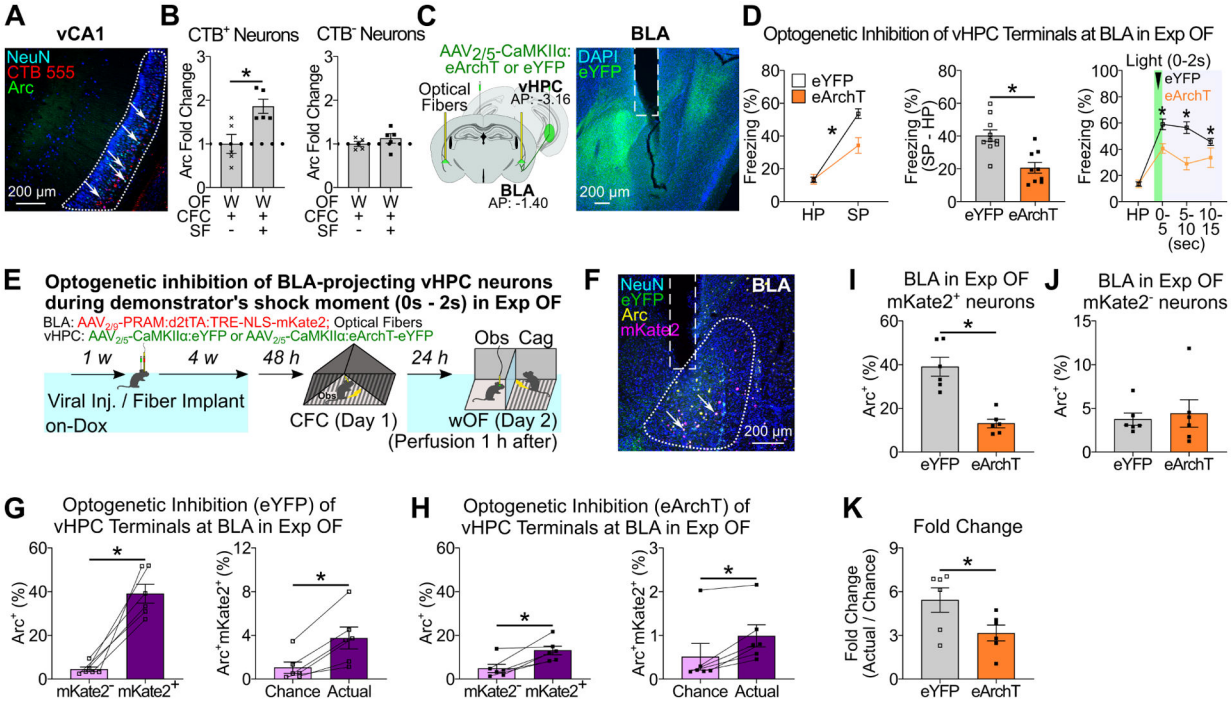

Figure 7. vHPC-BLA pathway in Exp OF.

(A) Coronal section of vHPC CA1. Arrows indicate $CTB^{+}Arc^{+}$ neurons. **(B)** Fold change analysis in the percentages of Arc^{+} neurons in CTB^{+} neurons (left) and CTB^{-} neurons (right) with stranger demonstrator (W/+/−) or cagemate demonstrator (W/+/+). Data are normalized by average of the stranger demonstrator (W/+/−) group. **(C)** (Left) Strategy. (Right) Coronal section of BLA. White lines indicate fiber implantation. **(D)** Observer freezing response with optogenetic vHPC terminal inhibition at BLA during the demonstrator's shock moment in Exp OF. (Left) Observer freezing levels during HP and SP of eYFP and eArchT groups. (Middle) Subtraction freezing levels. (Right) Observer freezing levels in post-shock bins in Exp OF. **(E)** Experimental schedule. **(F)** Coronal section of BLA with fiber implantation (white lines). Arrows; $Arc^{+}mKate2^{+}$ neurons. **(G-H)** (Left) Percentages of Arc^{+} neurons in $mKate2^{-}$ and $mKate2^{+}$ neurons in BLA of in eYFP (G) and eArchT (H) groups. (Right) Actual percentages and chance percentages of $Arc^{+}mKate2^{+}$ neurons in eYFP (G) and eArchT (H) groups. **(I-J)** Percentages of Arc^{+} neurons in $mKate2^{+}$ (I) or $mKate2^{-}$ (J) neurons of eYFP and eArchT groups. **(K)** Fold change analysis (actual / chance) comparing eYFP and eArchT groups. Graphs show means ± SEM. * $P < 0.05$ by two-sided unpaired t-test (B, D, I-K), and interaction with two-way mixed ANOVA (D), Mann-Whitney U-test (D), two-sided paired t-test (G-H). See also Supplemental Table 1 and Figure S12–13.

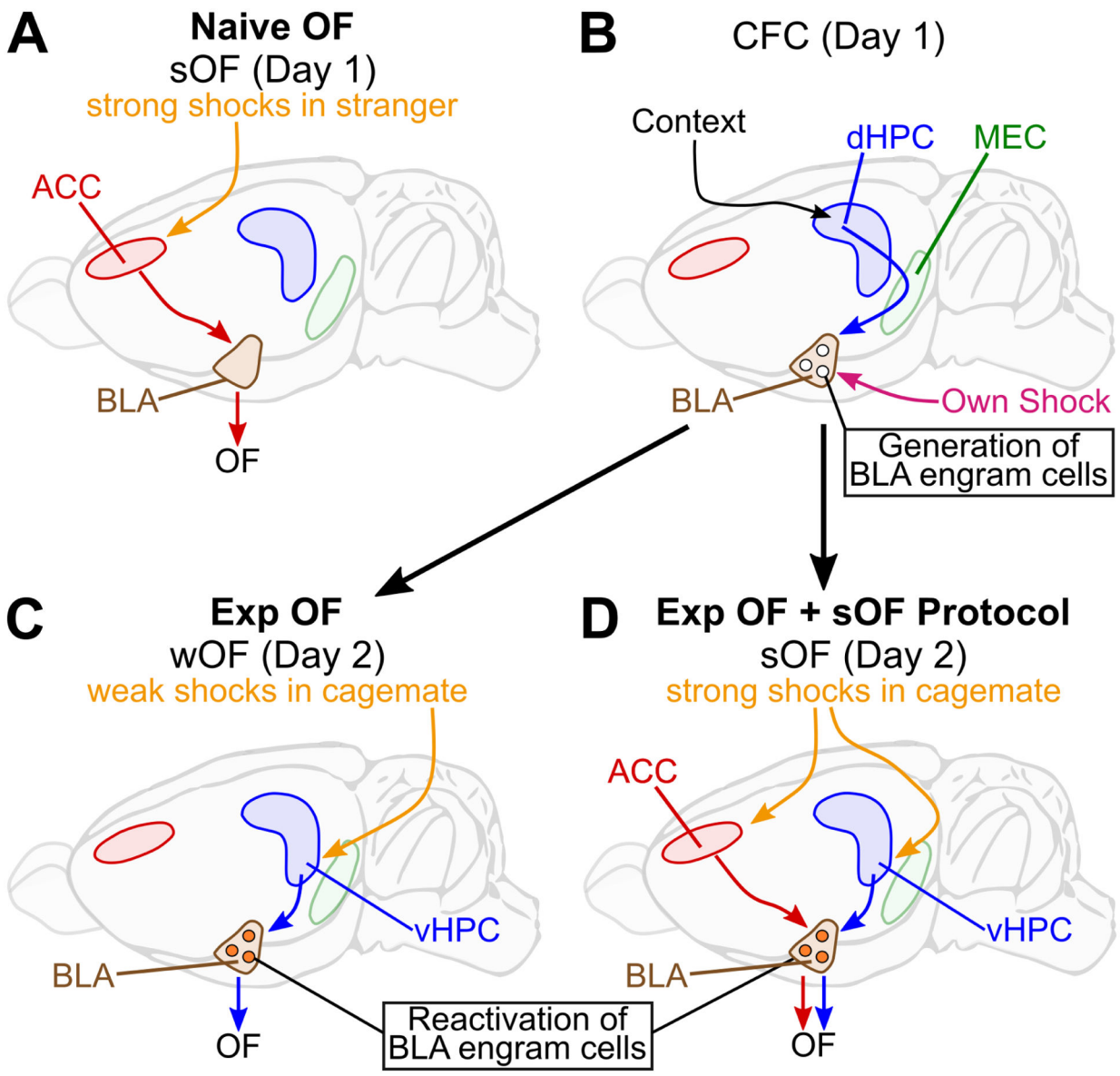

Figure 8. Proposed models for Naive OF and Exp OF.

(A) Strong shocks delivered to a stranger demonstrator activates the ACC to BLA pathway to facilitate Naive OF. **(B-C)** During prior CFC (contextual fear conditioning) experience on Day 1, dHPC via subiculum and/or medial entorhinal cortex (MEC) generates fear memory engram cells in BLA. On Day 2, when weak shocks are delivered to a cagemate demonstrator, BLA-projecting vHPC neurons reactivate BLA fear memory engram cells to facilitate Exp OF. **(B, D)** The combination of Exp OF (prior CFC experience on Day 1, exposure to OF with a cagemate demonstrator on Day 2) with the strong OF protocol (sOF) delivered to the demonstrator enhances OF response in observers. Both ACC and vHPC are necessary for Exp OF + sOF, which indicates that the ACC-BLA and HPC-BLA pathways parallelly facilitate OF. See also Supplemental Table S2 and Figure S14.

KEY RESOURCES TABLE

REAGENT or RESOURCE	SOURCE	IDENTIFIER
Antibodies		
Chicken polyclonal anti-NeuN	Millipore Sigma	Cat#:ABN191, RRID:AB_11205760
Chicken polyclonal anti-GFP	ThermoFisher Scientific	Cat#:A10262, RRID:AB_2534023
Guinea pig polyclonal anti-NeuN	Millipore Sigma	Cat#:ABN90, RRID:AB_11205592
Mouse monoclonal anti-HA	BioLegend	Cat#:901513, Clone ID: 16B12, RRID:AB_2565335
Mouse monoclonal anti-NeuN	Millipore Sigma	Cat#:MAB377, RRID:AB_2298772
Rabbit polyclonal anti-Arc	Synaptic Systems	Cat#:156003, RRID:AB_887694
Bacterial and Virus Strains		
rAAV-CaMKIIα-eArchT3.0-eYFP	UNC Vector Core	Cat#:AV4883
rAAV-CaMKIIα-eYFP	UNC Vector Core	Cat#:AV4808c
pAAV-CaMKIIα-hM4D(Gi)-mCherry	Bryan Roth (unpublished)	Cat#:50477, RRID:Addgene_50477
pAAV-CaMKIIα-mCherry	UNC Vector Core	Cat#:AV4809D
pAAV-PRAM-d2tTA:TRE-NLS-mKate2-WPREpA	Sorensen et al., *Elife*, 2016	Cat#:84474, RRID:Addgene_84474
pAAV-PRAM-d2tTA:TRE-HA-hM4D(Gi)-WPREpA	This paper	N/A
pENN.AAV.CamKII.GCaMP6f.WPRE.SV40	Penn Vector Core	Cat#100834, RRID:Addgene_100834
pAAV-hSyn-hM4D(Gi)-mCherry	Bryan Roth (unpublished)	Cat#:50475, RRID:Addgene_50475
pAAV-hSyn-mCherry	Karl Deisseroth (unpublished)	Cat#:114472, RRID:Addgene_114472
Chemicals, Peptides, and Recombinant Proteins		
Cholrea Toxin Subunit B, Alex Fluor 555	ThermoFisher Scientific	C22843
Clozapine N-Oxide	Enzo Life Sciences	BML-NS105-0025, CAS: 34233-69-7
Clozapine N-Oxide-dihydrochloride	HelloBio	HB6149, CAS: 2250025-93-3
DAPI (4’,6-Diamidino-2-Phenylindole, Dihydrochloride)	ThermoFisher Scientific	D1306, CAS: 28718-90-3
Dil	Biotium	Cat#60010, CAS: 41085-99-8
NMDA (N-Methyl-D-aspartic acid)	Sigma	M3262, CAS:6384-92-5
(RS)-CPP	Tocris	Cat#0173, CAS: 100828-16-8
VECTASHIELD® Antifade Mounting Medium	Vector Laboratories	H-1000, RRID:AB_2336789
Critical Commercial Assays		
In-Fusion HD Cloning Plus kit	Takara	638920
Experimental Models: Organisms/Strains		
C57BL/6J	Jackson Labs	Cat#:000664, RRID:IMSR_JAX:000664
Software and Algorithms		
Behavioral Observation Research Interactive Software (BORIS)	Friard & Gamba, Methods in Ecology and Evolution, 2016	http://www.boris.unito.it/, RRID:SCR_021434

REAGENT or RESOURCE	SOURCE	IDENTIFIER
Clampex 11.2	Molecular Devices	https://www.moleculardevices.com/products/axon-patch-clamp-system/acquisition-and-analysis-software/pclamp-software-suite, RRID:SCR_011323
Clampfit 11.2	Molecular Devices	https://www.moleculardevices.com/products/axon-patch-clamp-system/acquisition-and-analysis-software/pclamp-software-suite, RRID:SCR_011323
Custom MATLAB Code	This paper	https://zenodo.org/record/5838961, DOI: 10.5281/zenodo.5838961
ImageJ	NIH	https://imagej.nih.gov/ij/, RRID:SCR_003070
Inscopix Data Processing Software 1.2.1	Inscopix	N/A
MATLAB	MathWorks	https://www.mathworks.com/products/matlab.html?s_tid=hp_products_matlab, RRID:SCR_001622
Mosaic 1.2.0	Inscopix	RRID:SCR_017408
Prism 9	GraphPad	https://www.graphpad.com/scientific-software/prism/, RRID:SCR_002798
Video Freeze	Med Associates	https://www.med-associates.com/product/video-fear-conditioning/, SOF-843, RRID:SCR_014574
Zen Blue 2.3	Zeiss	https://www.zeiss.com/microscopy/int/products/microscope-software/zen.html,RRID:SCR_021725
Zen Lite	Zeiss	https://www.zeiss.com/microscopy/int/products/microscope-software/zen.html, RRID:SCR_021725
Other		
10 μL Microliter Syringe Model 701	Hamilton	80301
3-D Printed Custom-Designed Microdrive	This paper	N/A
532 nm Laser	Ultralasers	CST-w532–500mW
Axon Digidata 1550B	Molecular Devices	N/A
Baseplate	Inscopix	1050–004638
C&B Metabond Quick Adhesive Cement System	Parkell	S380
Capillary Borosilicate Glass 1.5mm OD, 0.84mm ID, 6 inch length, with filament	World Precision Instruments	1B150F-4
Dense Fabric Ball Attached to String	This paper	N/A
Digital Lynx 4SX	NeuraLynx	N/A
Doxyclyine mouse food 40 mg/kg, custom	Bio-serv	F5003
Elevated Platform for Unrelated Aversive Experience (Bright Light Illumination)	This paper	N/A
Function Generator	Siglent	SDG810
Inline Heater	Warner Instruments	SH-27B
Lecia VT1000 S Vibrating Blade Microtome	Leica	VT1000 S
Leica S6E Stereomicroscope	Leica	S6E
Microelectrode Holder (MPH6S)	World Precision Instruments	MPH6S10
MicroFil	World Precision Instruments	MF28G-5
Microinjection Syringe Pump	World Precision Instruments	UMP3T-1
Mono Fiber Optic Cannula	Doric Lenses	MFC_200/240-0.22_50mm_ZF1.25(G)_FLT

REAGENT or RESOURCE	SOURCE	IDENTIFIER
MultiClamp 700B Microelectrode Amplifier	Molecular Devices	N/A
NIR Video Fear Conditioning Package for Mouse	Med Associates	MED-VFC-OPTO-USB-M
NOA81 – Fast Curing Optical Adhesive	Norland	NOA81
nVoke v1.0	Inscopix	N/A
Observational Fear Apparatus	This paper	N/A
Pipette Puller	Narishige	PC-100
ProView Lens Probe	Inscopix	1050-004608
ProView Prism Probe	Inscopix	1050-004612
Single Channel Temperature Controller	Warner Instruments	TC-324C
Small Animal Stereotaxic Instrument with Digital Display Console	David Kopf Instruments	Model 942
UV Curing LED System, 365 nm	ThorLabs	CS2010
Wiretrol® I	Drummond Scientific Company	5-000-1001-X
Zeiss Axio Examiner A1	Zeiss	N/A
Zeiss AxioImager M2 with Apotome	Zeiss	N/A
Zeiss LSM800 with Airyscan	Zeiss	N/A